

THE RESOLVED PROPERTIES OF EXTRAGALACTIC GIANT MOLECULAR CLOUDS

ALBERTO D. BOLATTO¹, ADAM K. LEROY², ERIK ROSOLOWSKY^{3,4}, FABIAN WALTER², & LEO BLITZ⁵*Draft version February 10, 2022*

ABSTRACT

We use high spatial resolution observations of CO to systematically measure the resolved *size-line width*, *luminosity-line width*, *luminosity-size*, and the *mass-luminosity* relations of Giant Molecular Clouds (GMCs) in a variety of extragalactic systems. Although the data are heterogeneous we analyze them in a consistent manner to remove the biases introduced by limited sensitivity and resolution, thus obtaining reliable sizes, velocity dispersions, and luminosities. We compare the results obtained in dwarf galaxies with those from the Local Group spiral galaxies. We find that extragalactic GMC properties measured across a wide range of environments are very much compatible with those in the Galaxy. The property that shows the largest variability is their resolved brightness temperature, although even that is similar to the average Galactic value in most sources. We use these results to investigate metallicity trends in the cloud average column density and virial CO-to-H₂ factor. We find that these measurements do not accord with simple predictions from photoionization-regulated star formation theory, although this could be due to the fact that we do not sample small enough spatial scales or the full gravitational potential of the molecular cloud. We also find that the virial CO-to-H₂ conversion factor in CO-bright GMCs is very similar to Galactic, and that the excursions do not show a measurable metallicity trend. We contrast these results with estimates of molecular mass based on far-infrared measurements obtained for the Small Magellanic Cloud, which systematically yield larger masses, and interpret this discrepancy as arising from large H₂ envelopes that surround the CO-bright cores. We conclude that GMCs identified on the basis of their CO emission are a unique class of object that exhibit a remarkably uniform set of properties from galaxy to galaxy.

Subject headings: galaxies: ISM — ISM: clouds — galaxies: dwarf — galaxies: individual (IC 10, M 31, M 33, NGC 185, NGC 205, NGC 1569, NGC 2976, NGC 3077, NGC 4214, NGC 4449, NGC 4605) — Magellanic Clouds

1. INTRODUCTION

Giant Molecular Clouds (GMCs) are the major reservoirs of molecular gas and the sites of most star formation in our Galaxy and other galaxies. Their properties set the initial conditions for protostellar collapse, and may play a role in determining the stellar initial mass function (McKee & Ostriker 2007). Moreover, because GMCs provide the bulk of the material for forming new stars their creation may be the limiting mechanism that regulates the rate of star formation in galaxies. Therefore, increasing our understanding of their properties and distribution throughout the different environments of external galaxies is likely to provide further insights into GMC and stellar formation processes. There is a limited amount of information, however, that can be gained from studies that resolve the general distribution of molecular gas but not the individual molecular clouds. Resolving GMCs — to measure their sizes, velocity dispersions, and luminosities — is a critical step in understanding the processes that ultimately drive galaxy evolution.

Studies of resolved molecular clouds in the Milky Way find that GMCs are in approximate virial equilibrium and obey scaling relations, commonly known as Larson laws (Larson 1981), that have their origin in the character of the turbulence in the interstellar medium (Elmegreen & Scalo 2004; McKee & Ostriker 2007). Large scale surveys of the Milky Way show that GMCs follow uniform scaling relations (Solomon et al. 1987; Elmegreen & Falgarone 1996), with few differences present between those located in the inner and the outer disk (Heyer, Carpenter, & Snell 2001).

Larson (1981) established that velocity dispersion, size, and luminosity are correlated in Milky Way GMCs. Observations indicate that GMC line widths increase as a power of their radius (Solomon et al. 1987), such that

$$\sigma_v \approx 0.72 R^{0.5} \text{ km s}^{-1}, \quad (1)$$

where σ_v is the one-dimensional velocity dispersion of the GMC, and R is its radius measured in parsecs. Equation 1 is known as the *size-line width* relation, and it has been shown to hold even within GMCs down to very small scales (Heyer & Brunt 2004; Rosolowsky et al. 2008).

The *size-line width* relation is an expression of the equilibrium turbulence conditions in the molecular ISM. Detailed modeling of GMC line profiles shows that the emission is macroturbulent (i.e., the scale size of the turbulence is larger than the photon mean free path), corresponding to many optically thick clumps that have a clump-to-clump velocity dispersion similar to the observed line width (Wolfire et al. 1993). It is known that

Electronic address: bolatto@astro.umd.edu

¹ Department of Astronomy and Laboratory for Millimeter-wave Astronomy, University of Maryland, College Park, MD 20742, USA

² Max-Planck-Institut für Astronomie, D-69117 Heidelberg, Germany

³ Harvard-Smithsonian Center for Astrophysics, Cambridge, MA 02138, USA

⁴ Department of Mathematics, Statistics, and Physics, University of British Columbia at Okanagan, Kelowna, B.C. V1V 1V7, Canada

⁵ Department of Astronomy and Radio Astronomy Laboratory, University of California at Berkeley, Berkeley, CA 94720, USA

the observed line widths in all but a few very compact, quiescent clouds are too large to be thermal; at the typical GMC temperatures of 15 – 25 K the thermal CO velocity dispersion would be $\lesssim 0.1 \text{ km s}^{-1}$. They are rather due to supersonic turbulence within the clouds. The dominant sources of turbulence in the molecular ISM remain somewhat controversial. For example, it is not yet known whether turbulence in molecular clouds is primarily internally or externally driven (e.g., McKee & Ostriker 2007). Contributors must include star formation — in the form of jets and winds for low mass stars, and winds and expanding HII regions for massive stars — and star destruction — in the form of supernovae shocks and expanding superbubbles. Global processes that couple the large reservoirs of thermal or rotational energy to the turbulent cascade — such as spiral shocks and several types of instabilities that involve shear, magnetic fields, and self gravity — are important on the largest spatial scales. The fact that turbulence is present on scales $\gtrsim 100 \text{ pc}$ (e.g., Brunt 2003; Dib & Burkert 2005), and that the dissipation lifetime of the largest eddies is $\lesssim 10^7 \text{ yr}$ (Fleck 1981; Stone, Ostriker, & Gammie 1998), point to constant (or at least frequent) energy injection on large scales. This in turn suggests that massive stellar death and global mechanisms are predominantly responsible for the bulk of turbulent energy injection in the Milky Way, although their respective dominance is a matter of debate (MacLow 2004; Piontek & Ostriker 2004, 2005).

The last two Larson relations, the *luminosity-line width* and *luminosity-size* relations, describe correlations between cloud luminosity, L_{CO} , and either velocity dispersion or size (note, as is frequently pointed out, that only two of the three Larson relations are independent). They are (Solomon et al. 1987)

$$L_{\text{CO}} \approx 130 \sigma_v^5 \text{ K km s}^{-1} \text{ pc}^2, \quad (2)$$

and

$$L_{\text{CO}} \approx 25 R^{2.5} \text{ K km s}^{-1} \text{ pc}^2, \quad (3)$$

with σ_v and R expressed in their corresponding units of km s^{-1} and pc .

Thus, the observations show that the virial mass, M_{vir} , relates to the CO luminosity (which is proportional to the inferred luminous mass M_{lum}) in the following manner (Solomon et al. 1987),

$$M_{\text{vir}} \approx 39 L_{\text{CO}}^{0.81} M_{\odot} \quad (4)$$

where L_{CO} is expressed in $\text{K km s}^{-1} \text{ pc}^2$. We will call this equation the Galactic *mass-luminosity* relation. Note that the exponent of L_{CO} is somewhat uncertain, and we take here the value reported by Solomon et al.. Although the relation may not be precisely linear it is almost so, and simple models of molecular clouds can explain the observed linearity (Dickman, Snell, & Schloerb 1986). This approximate proportionality between L_{CO} and M_{vir} within the Galaxy allows the definition of an empirical CO-to- H_2 conversion factor, X_{CO} , that relates the intensity of a GMC in the $^{12}\text{CO } J = 1 \rightarrow 0$ transition to its H_2 column density ($N(\text{H}_2) = X_{\text{CO}} I_{\text{CO}}$) and ultimately its mass. For GMCs around a median mass of $5 \times 10^5 M_{\odot}$ Solomon et al. obtained a CO-to- H_2 factor

that, when adjusted to the currently accepted distance of 8.5 kpc to the Galactic Center, yields $X_{\text{CO}} \approx 1.9 \times 10^{20} \text{ cm}^{-2} (\text{K km s}^{-1})^{-1}$ (McKee & Ostriker 2007). In the Milky Way, this “virial mass” approach yields conversion factors similar to those obtained from non-dynamical measurements, strongly suggesting that clouds are in a dynamical state intermediate between marginal gravitational binding and virial equilibrium (e.g., γ -ray results and modeling of the Galactic plane dust continuum; Bloemen et al. 1984; Strong & Mattox 1996; Dame, Hartmann, & Thaddeus 2001), with magnetic energy introducing a small but non-negligible correction on the small scales ($\lesssim 50\%$; Crutcher 1999). Throughout this paper we adopt $X_{\text{CO}} = 2 \times 10^{20} \text{ cm}^{-2} (\text{K km s}^{-1})^{-1}$ as the Galactic conversion factor. Note, however, that some nearby lines-of-sight at high Galactic latitudes may exhibit significant larger values of this coefficient (e.g., Magnani, Blitz, & Wouterloot 1988; Grenier, Casandjian, & Terrier 2005).

Therefore, mass estimates of GMCs show that they are gravitationally bound and in approximate virial equilibrium, which requires $M_{\text{vir}} \sim R \sigma_v^2 \propto M_{\text{lum}}$. As a consequence of Equation 1 and virial equilibrium, all GMCs have approximately the same mean column density: $N_{\text{H}} \approx 1.5 \times 10^{22} \text{ cm}^{-2}$, or an equivalent mass surface density $\Sigma \approx 170 M_{\odot} \text{ pc}^{-2}$ (after applying a 40% correction for the mass contribution of elements heavier than Hydrogen). An equivalent result is that all Milky Way GMCs have approximately the same mean visual extinction from edge to edge, $A_V \sim 7.5$, using the standard dust-to-gas ratio (Bohlin, Savage, & Drake 1978).

McKee (1999) argues that Equation 4 is a consequence of the interplay between CO chemistry, the Milky Way radiation field, the dust-to-gas ratio, and the local pressure of the ISM. As a result, H_2 clouds observable in CO are at least marginally bound. Furthermore, McKee argues that the constancy of N_{H} stems from the fact that clouds with lower column density would not be bright in CO, while clouds with higher column density would rapidly collapse.

Another consequence of the Larson relations is that Galactic GMCs have low volume-averaged densities, $50 < n(\text{H}_2) < 500 \text{ cm}^{-3}$. Therefore their clumpiness must be high in order to excite the rotational transitions of CO and of other commonly observed high-density tracer molecules such as HCO^+ , which require volume densities in excess of 10^4 cm^{-3} . This clumpiness is probably induced by supersonic turbulence (Padoan et al. 1998; Ostriker, Gammie, & Stone 1999). Further, the average density of a GMC decreases with increasing mass, and as a result the free fall time in the cloud increases. This led Krumholz & McKee (2005) to predict that larger GMCs will form collapsing cores and stars less rapidly than smaller ones.

The purpose of this study is to determine, *using a consistent methodology*, the relations between size, velocity dispersion, and luminosity for extragalactic GMCs that are encapsulated in the Milky Way by the Larson laws. We do so by studying GMCs in dwarf galaxies and comparing them with those in spiral galaxies. Dwarf galaxies are both numerous and nearby, and host physical conditions that fall outside those explored by surveys of the Milky Way. The range of parameter space thus

probed provides an ideal laboratory to test theories of cloud structure and formation. Particularly, dwarf galaxies have low metallicities and their lack of internal extinction results in intense radiation fields, reminiscent of the conditions in primitive galaxies. They display irregular morphologies and are not dominated by spiral structure. Dwarfs often have slowly rising, nearly solid-body, rotation curves; this translates into small rotational shear and perhaps changes the sources and scales of turbulence in their ISM. The stellar potential wells of dwarf galaxies are weaker than those in large spiral galaxies and the ambient ISM may be correspondingly less dense. These environmental changes may influence the equilibrium conditions of GMCs, and affect their Larson relations.

The integrated properties of dwarf galaxies already show clear evidence that environment affects at least the CO content. Dwarf irregular galaxies are fainter in CO than large spiral galaxies. Galaxies with metallicity $12 + \log \text{O}/\text{H} \lesssim 8.0$ are seldom detected in CO emission (Taylor et al. 1998). Dwarf galaxies of higher metallicity detected in CO, however, show similar CO luminosity relative to either their stellar or atomic gas content as larger galaxies (Leroy et al. 2005). Here we investigate whether the resolved properties of GMCs in these galaxies also reflect their changing environments.

1.1. Resolving extragalactic molecular clouds

The study of resolved GMC properties in other galaxies remains technically challenging. A typical size for a Galactic GMC is ~ 40 pc, which at the ~ 4 Mpc distance of the M 81 group translates to an angular size of $\sim 2''$. Achieving such a resolution requires an antenna 250 meters in diameter operating at $\lambda = 2.6$ mm, the wavelength of the ground transition of ^{12}CO . This is clearly an impractical proposition, but aperture synthesis techniques used by millimeter-wave interferometers routinely attain this resolution. They do so, however, at the price of reduced surface brightness sensitivity with respect to their filled aperture equivalents, and studies such as the one presented here are ultimately limited by sensitivity. Until the advent of the Atacama Large Millimeter Array (ALMA) these observations will remain challenging.

Because of these difficulties, the resolved properties of GMCs in galaxies other than the Milky Way remain a largely unexplored domain. Because of its proximity, located at a distance where even a modest telescope can attain a resolution of $\sim 30 - 40$ pc, the first galaxy where observations capable of clearly resolving individual GMCs were possible was the Large Magellanic Cloud (Israel et al. 1982). The first resolved study of a GMC beyond the immediate vicinity of the Milky Way was performed in M 31 (Vogel, Boulanger, & Ball 1987), while the first large scale interferometric survey of GMCs in another galaxy was done on M 33 (Wilson & Scoville 1990). The first comprehensive analyses in the Magellanic Clouds were performed on the Small Magellanic Cloud (Rubio et al. 1991; Rubio, Lequeux, & Boulanger 1993b).

Blitz et al. (2007) recently presented a study of GMCs in the Local Group, analyzing observations from CO surveys complete down to a known mass limit over a significant fraction of each galaxy. This study concluded that the Larson relations in the Milky Way disk were approximately those observed throughout the Local

Group, although some offsets (possibly methodological) were present. They also concluded that GMCs within a particular galaxy have roughly constant surface density, Σ_{GMC} , and that once corrections for the local CO-to- H_2 conversion factor are applied the sample as a whole has a scatter of only a factor of 2 in Σ_{GMC} . Finally, they calculated a typical conversion factor $X_{\text{CO}} \approx 4 \times 10^{20} \text{ cm}^{-2} (\text{K km s}^{-1})^{-1}$, accurate to within 50% for most of the sample except the Small Magellanic Cloud, for which they obtain a value ~ 3 times larger.

This paper proceeds as follows: in §2 we describe the data sets and the galaxies studied. In §3 we summarize the method used to consistently derive GMC properties across the different datasets. In §4 we discuss the *size-line width*, *luminosity-line width*, and *luminosity-size* relations in our sample of extragalactic GMCs, and compare them with the Galaxy. In §5 we discuss the implications of these results on the equilibrium of clouds in the Small Magellanic Cloud, the photoionization-regulated star formation theory, the CO-to- H_2 conversion factor, and the brightness temperature of extragalactic clouds. In each case we contrast our results in dwarf galaxies with those obtained in the Milky Way and the other Local Group spirals, M 31 and M 33. In §6 we summarize this study and present our conclusions.

2. DATA

We use data from four telescopes: the Berkeley-Illinois-Maryland Array (BIMA; Welch et al. 1996), Caltech’s Owens Valley Radio Observatory (OVRO) millimeter array, the Institut de Radioastronomie Millimétrique Plateau de Bure Interferometer (PdBI), and the Swedish-ESO Submillimeter Telescope (SEST). We measure GMC properties in 11 dwarf galaxies: the Large and Small Magellanic Clouds, IC 10, NGC 185, NGC 205, NGC 1569, NGC 2976, NGC 3077, NGC 4214, NGC 4449, and NGC 4605. We compare GMC properties derived in dwarfs to those found in the Milky Way (data obtained by the Five Colleges Radio Astronomy Observatory, FCRAO; Sanders et al. 1986) and the other two Local Group spiral galaxies, M 31 and M 33. The latter two act as key “control” data sets because they are obtained by the same telescopes at similar angular and spatial resolutions to the dwarf galaxy GMC data. Table 1 gives the source, telescope, line observed, resolutions, and reference for each data set.

When we analyze observations of the CO $J = 2 \rightarrow 1$ transition, we assume $I(2 \rightarrow 1) = I(1 \rightarrow 0)$ (i.e., thermalized optically thick emission). For the GMC complex in the N83 region of the Small Magellanic Cloud, this is within 10% of the observed ratio (Bolatto et al. 2003). In the Milky Way the observed ratio varies from unity to $I(2 \rightarrow 1) \sim 0.65 I(1 \rightarrow 0)$ (e.g., Sawada et al. 2001).

Several data sets appear here for the first time. Notably, GMCs in NGC 3077, NGC 4214, and NGC 4449 where mapped at BIMA as part of a large project studying the molecular ISM in dwarf galaxies. The BIMA maps of NGC 2976 and NGC 4605 were obtained as part of the same project and have appeared previously in kinematic analyses (Bolatto et al. 2002; Simon et al. 2003). The observation and reduction procedure for these data follow the descriptions in those papers.

Table 2 lists the properties of the galaxies that we study. Most have late type morphologies; the exceptions

TABLE 1
DATA SETS USED IN THIS PAPER

Source	Instr.	Transition	Resol. (pc)	Resol. (km s ⁻¹)	Ref.
IC 10	OVRO	1 → 0	19	0.7	5
NGC 185	BIMA	1 → 0	15	4	1
NGC 205	BIMA	1 → 0	28	3	1
SMC N83	SEST	2 → 1, 1 → 0	11, 17	0.25	9
SMC LIRS36	SEST	2 → 1	7	0.05	10
SMC LIRS49	SEST	2 → 1	7	0.05	10
LMC N159	SEST	2 → 1	6	0.25	11
NGC 1569	PdBI	2 → 1, 1 → 0	22, 45	1.6	8
NGC 2976	BIMA	1 → 0	94	3	2
NGC 3077	BIMA	1 → 0	41	3	3
NGC 3077	OVRO	1 → 0	41	1.3	6
NGC 4214	BIMA	1 → 0	80	3	3
NGC 4214	OVRO	1 → 0	64	1.3	7
NGC 4449	BIMA	1 → 0	117	3	3
NGC 4605	BIMA	1 → 0	109	3	4

Disk Galaxies					
Milky Way	FCRAO	1 → 0	3 – 11	0.65	12
M 31	BIMA	1 → 0	27	2	14
M 33	BIMA	1 → 0	30	2	13

REFERENCES. — (1) Young (2001); (2) Simon et al. (2003); (3) This Work; (4) Bolatto et al. (2002); (5) Walter (2003); (6) Leroy et al. (2006); (7) Walter et al. (2002); (8) Taylor et al. (2001); (9) Bolatto et al. (2003); (10) Rubio et al. (1993a); (11) Bolatto et al. (2000); (12) Sanders et al. (1986); (13) Rosolowsky et al. (2003); (14) Rosolowsky (2007)

are NGC 185 and NGC 205, Local Group dwarf ellipticals mapped by Young (2001) using BIMA. All of our sources are < 5 Mpc away; the most distant galaxy is NGC 4605 at 4.26 Mpc. We indicate the absolute blue magnitude of each galaxy corrected by Galactic extinction to illustrate their luminosity. The galaxies span the range $-18 \lesssim M_B \lesssim -15$ magnitudes. We give metallicities for each galaxy, with the corresponding references for metallicity and distance.

2.1. Dwarf Galaxies

In this section we briefly summarize the sources and datasets used. For more in-depth descriptions we point the reader to the original references.

Young (2001) used the BIMA interferometer to map CO $J = 1 \rightarrow 0$ emission in the Local Group dwarf elliptical galaxies NGC 185 and NGC 205. These galaxies, which are satellites of M 31, are unusual early-type dwarfs with CO emission, while the rest of our sample consists of late-type dwarf spiral and irregular galaxies.

Simon et al. (2003) presented a kinematic study based on BIMA observations of CO $J = 1 \rightarrow 0$ emission from NGC 2976, a dwarf spiral galaxy in the M 81 group. These observations are considerably deeper than those from the BIMA Survey of Nearby Galaxies (SONG; Helfer et al. 2003). The metallicity for this galaxy is uncertain, but the polycyclic aromatic hydrocarbon abundance and dust-to-gas ratios derived by Draine et al. (2007) suggests it is similar to Galactic.

Walter et al. (2002) mapped CO $J = 1 \rightarrow 0$ emission from NGC 3077, a member of the M 81 group cur-

TABLE 2
GALAXY PROPERTIES

Galaxy	Morph.	Dist.	M_B	Met.	Ref.
IC 10	Irr/BCD	0.95	-16.7	8.2	6,19
NGC 185	dSph/dE3	0.63	-14.7	8.2	1,17
NGC 205	E5	0.85	-15.9	8.6	1,18
SMC	Sm	0.061	-16.7	8.02	7,20
LMC	Sm	0.052	-18.0	8.43	7,20
NGC 1569	Irr	2.2	-17.3	8.19	2,16
NGC 2976	Sc	3.45	-17.4	8.7	3,13
NGC 3077	Irr	3.9	-17.5	8.85	3,11
NGC 4214	Irr	2.94	-17.2	8.23	4,12
NGC 4449	Irr	3.9	-18.0	8.32	5,15
NGC 4605	Sc	4.26	-17.9	8.69	3,14

Large Galaxies					
Milky Way	SB	0.008	-21.4	8.7	10
M31	Sb	0.79	-21.1	8.7	8,21
M33	Scd	0.84	-18.9	8.4	9,21

REFERENCES. — (1) Richer & McCall (1995); (2) Kobulnicky & Skillman (1997); (3) This work. See §2.1; (4) Kobulnicky & Skillman (1996); (5) Skillman et al. (1989); (6) Lequeux et al. (1979); (7) Dufour (1984); (8) Pilyugin et al. (2004); (9) Rosolowsky & Simon (2007); (10) Baumgartner & Mushotzky (2006); (11) Sakai & Madore (2001); (12) Maíz-Apellániz, Cieza, & MacKenty (2002); (13) Simon et al. (2003); (14) Bolatto et al. (2002); (15) Hunter et al. (2005); (16) Israel (1988); (17) Martínez-Delgado & Aparicio (1998); (18) Salaris & Cassisi (1998); (19) Hunter (2001); (20) Keller & Wood (2006); (21) Kennicutt et al. (1998)

NOTE. — Distances are in Mpc. Luminosities are corrected for Galactic extinction. Metallicities are expressed as $12 + \log O/H$.

rently undergoing a dramatic interaction with M 81 and M 82, using the OVRO millimeter interferometer. This galaxy was also observed by BIMA during the same period, and those observations appear here for the first time. We present GMC property measurements from both data sets. We derive the metallicity for this galaxy using the integrated nebular fluxes of the bright oxygen lines by Moustakas & Kennicutt (2006), employing the calibration of McGaugh (1991) as parametrized by Kobulnicky, Kennicutt, & Pizagno (1999). The metallicity is consistent with that derived using the nitrogen calibration by Kewley & Dopita (2002).

Walter et al. (2001) mapped CO $J = 1 \rightarrow 0$ emission from NGC 4214, a nearby dwarf irregular galaxy, using the OVRO millimeter interferometer. This galaxy was also observed by BIMA, and here we use those data for the first time.

BIMA mapped CO $J = 1 \rightarrow 0$ emission from the nearby dwarf irregular NGC 4449. The data appear here for the first time.

Bolatto et al. (2002) presented CO $J = 1 \rightarrow 0$ observations of NGC 4605, a nearby isolated dwarf galaxy, and used them to study the kinematics of this galaxy. The metallicity for this galaxy was derived using the same procedure as for NGC 3077.

Walter (2003) mapped CO $J = 1 \rightarrow 0$ emission from most of the molecular clouds in the Local Group dwarf irregular IC 10 using the OVRO millimeter interferometer. These data were analyzed in detail by Leroy et al. (2006), where maps of individual GMCs are presented. IC 10 is a Local Group irregular comparable in mass to

the Small Magellanic Cloud but presently undergoing a burst of vigorous star formation.

Taylor et al. (1999) used the PdBI to map both CO $J = 2 \rightarrow 1$ and $J = 1 \rightarrow 0$ emission from the nearby dwarf irregular NGC 1569. This galaxy, which is about the mass of the Small Magellanic Cloud, experienced a starburst period that ended ~ 5 Myr ago.

Bolatto et al. (2003) presented high signal-to-noise mapping of the N83 region in the Small Magellanic Cloud (SMC) using the SEST telescope. They observed both the CO $J = 2 \rightarrow 1$ and $J = 1 \rightarrow 0$ transitions. N83/N84 is a bright star forming region in the eastern wing of the Small Magellanic Cloud.

Bolatto et al. (2000) used SEST to map CO $J = 2 \rightarrow 1$ emission in the N159 region of the Large Magellanic Cloud (LMC). This region lies just south of the bright star forming region 30 Doradus, and comprises clouds in different stages of evolution.

2.2. Large Galaxies

In this study we use GMCs properties measured in the spiral disk galaxies of the Local Group as comparison and control datasets. As discussed in the introduction, several studies have established the scalings for Galactic molecular clouds (Larson 1981; Solomon et al. 1987; Elmegreen & Falgarone 1996; Heyer et al. 2001; Heyer & Brunt 2004; Rosolowsky et al. 2008). Recent interferometric work has shown that the GMCs in the other disk galaxies in the Local Group (M 31 and M 33) follow the same scalings (Wilson & Scoville 1990; Rosolowsky et al. 2003; Rosolowsky 2007; Sheth et al. 2008).

The observations of GMCs in M 33 employed here were made using the BIMA millimeter interferometer and are presented by Rosolowsky et al. (2003). That study analyzed 20 fields in that galaxy with a resolution $\theta \sim 6'' \sim 20$ pc, targeting sources identified in the all-disk survey of Engargiola et al. (2003). The M 31 GMCs belong to a region along the northwest spiral arm of this galaxy, also observed by BIMA (Rosolowsky 2007). This region was chosen for its favorable observing geometry, strong dust lanes and active star formation. Both studies concluded that the GMCs in these disks were indistinguishable in their aggregate properties from the clouds in the inner Milky Way. These observations constitute the most complete data sets for these galaxies, have sensitivity and resolution comparable to the dwarf galaxy data, and have been analyzed in an identical fashion.

For the Milky Way we employ the catalog of GMC properties by Solomon et al. (1987). This catalog consists of size, line width, and luminosity measurements for 273 Galactic GMCs and constitutes a representative data set of Milky Way GMC properties. Like us (see §3), Solomon et al. use moments to measure cloud properties and isosurface-based methods to identify individual GMCs. Their study, however, does not make an explicit correction for the effects of sensitivity (they use boundary isosurfaces of brightness temperature $T_B = 4$ to 7 K). It also uses an outdated Galactocentric distance for the Sun (10 kpc). It is unclear how to best correct their catalogued cloud properties to bring them into closer agreement with our methodology. We use here the original numbers, and rely on the M 31 and M 33 data as a consistency check. As is apparent in Figures 1, 2, and

3, these data are in good agreement with the standard Larson relations derived for the Milky Way sample.

3. METHODOLOGY

The challenge of any study that uses different instruments to study galaxies with a range of intrinsic properties and distances is to control the systematic biases introduced by the differences in the datasets. We measure cloud properties using the algorithm described in detail by Rosolowsky & Leroy (2006) and summarized here. This method measures luminosities, line widths, and sizes of GMCs in a manner that minimizes the biases introduced by signal-to-noise and resolution. These biases are the Achilles heel of comparisons of GMC measurements across different galaxies obtained by different telescopes. Rosolowsky & Leroy proposed that moment measurements combined with beam deconvolution and extrapolation represent a robust way to compare heterogeneous observations of molecular clouds. The algorithm is part of a package called CPROPS implemented in IDL and is available upon request. The remainder of this section summarizes the approach step-by-step.

The robustness, reliability, and consistency of the CPROPS methodology was tested by Rosolowsky & Leroy (2006) for a globally applicable set of algorithm parameters. They found the algorithm performed very well for data with signal-to-noise ratios (S/N) $\gtrsim 10$, but cautioned that measurements of the properties of GMCs observed with low S/N remain uncertain, particularly when using the default set of algorithm parameters. Unfortunately, CO is faint in dwarf galaxies, which makes it difficult to attain the optimal combination of S/N and spatial resolution. Therefore, only a few of the datasets discussed here meet the $S/N \geq 10$ criterion. Nevertheless, the data assembled here represent the best observations of GMCs in dwarf galaxies to date. As a consequence of the low S/N data, we made minor adjustments described below to the standard CPROPS parameters to improve the reliability of our results.

3.1. Identify Signal In Each Data Set

First, we identify regions of significant emission in each data set. For most of our data these are defined as regions that contain pixels which satisfy the condition of having 3 consecutive velocity channels above 4σ significance (i.e. a high significance “core”). We extend these regions to include all adjacent data which has at least 2 consecutive channels above 1.5σ significance. For a few data sets this did not yield the best results and we adjusted either the core or the edge conditions: a higher edge threshold was used in the high S/N N83 and N159 data sets; lower core thresholds were needed for the low S/N NGC 185 and NGC 205 data sets; a few other minor adjustments were also made. These changes yielded stable properties for clouds of low S/N, and suppressed diffuse emission blending clouds together in the extremely high S/N case. The signal identification step, often referred to as “masking”, can have a large impact on derived cloud properties and is difficult to motivate physically, especially in the low S/N regime common to much of our data. Thus, by necessity this step introduces a certain amount of subjectivity in the analysis.

3.2. Apportion Emission Into Clouds

Once signal is identified, data is apportioned into individual clouds following Rosolowsky & Leroy (2006). In all cases, we use the “physical priors” described in their appendix, which set the parameters of the decomposition to common values motivated by the properties of Galactic GMCs. This entails decomposing emission into clouds using effective spatial and velocity resolutions of 15 pc and 2 km s^{-1} and ignoring even high-contrast substructure below these scales. When it is not possible to achieve these resolutions because of limitations in the data, we use the actual spatial or velocity resolution of the observations. When two potential clouds share an isosurface, the algorithm adopts a conservative approach to separating them. The clouds are considered separate only if all of the following conditions are met: 1) each is large enough to measure meaningful properties, 2) each shows a minimum contrast between peak and edge, and 3) the decision to break the isosurface into multiple clouds has a significant effect on the derived cloud properties. Rosolowsky & Leroy (2006) showed this approach to be conservative and robust in the presence of noise, minimizing the identification of low-signal, marginally resolved (and thus often spurious) clouds.

3.3. Use Moments to Measure Cloud Properties

After identifying the individual clouds, we calculate their size, velocity dispersion, and CO luminosity. We determine the major and minor axis of the cloud using principal component analysis and measure the second moments of emission distribution along these axes. The RMS size of the cloud (σ_r) is the geometric mean of these two moments. The velocity dispersion (σ_v) is measured from the second moment along the velocity axis, and the luminosity via the zeroth moment (sum) over the cloud.

At finite signal-to-noise the second moment will underestimate the true cloud size, introducing a sensitivity bias. Although for Galactic data it is possible to measure reliable properties by adopting a fixed brightness boundary for clouds (e.g., Solomon et al. 1987), it would be impossible to compare measurements of different galaxies without removing this bias. We avoid the sensitivity bias by measuring the size, velocity, and luminosity as a function of intensity isosurface and extrapolating this to the case of infinite signal-to-noise. The size and line width of the cloud are extrapolated linearly, the luminosity is extrapolated quadratically (see Rosolowsky & Leroy 2006, for a justification of the extrapolation orders). We discussed in §2.2 the corrections that we apply to the Galactic sample to bring it into agreement with our methodology.

It is often the case for extragalactic observations that the size and line width of a GMC are comparable to the angular and velocity resolution of the telescope. We correct for this by “deconvolving” both the telescope beam and the velocity channel profile. We do so by subtracting their values from the extrapolated moment measurements in quadrature. Clearly this step does not come for free in signal-to-noise. Size measurements of clouds that are only marginally resolved suffer from substantial uncertainty, and this is accounted for in the error estimates.

3.4. Derive Physical Quantities

From the moment measurements we convert to physical units — radius, luminous mass, virial mass. The velocity dispersion is given directly by the moment.

We convert the RMS size to the spherical radius of the cloud using the factor $3.4/\sqrt{\pi}$, so that radii in this paper follow the Solomon et al. (1987) definition: $R = 1.91\sigma_r$. This factor can be motivated by considering a constant density spherical cloud and comparing its RMS size to its radius.

We compute luminous masses, M_{lum} , using the formula

$$M_{lum} = 1.1 \times 10^4 S_{CO} D^2 M_{\odot}, \quad (5)$$

where $S_{CO} \equiv \int I_{CO} d\Omega dv$ is the integrated ^{12}CO flux of the molecular cloud measured in Jy km s^{-1} , D is the distance to the source in Mpc, and the coefficient corresponds to our adopted conversion factor $X_{CO} = 2 \times 10^{20} \text{ cm}^{-2} (\text{K km s}^{-1})^{-1}$, and includes the contribution of the cosmological He abundance to the total mass. Equivalently, for a CO luminosity L_{CO} expressed in $\text{K km s}^{-1} \text{ pc}^2$,

$$M_{lum} = 4.5 L_{CO} M_{\odot}. \quad (6)$$

We compute the virial masses under the assumption that each cloud is spherical and virialized with a density profile of the form $\rho \propto r^{-1}$. This assumption is made for consistency with previous work, and we cannot assess its validity with the data in hand. Thus the virial mass is given by the formula (Solomon et al. 1987)

$$M_{vir} = 1040 \sigma_v^2 R M_{\odot}, \quad (7)$$

where σ_v is the cloud velocity dispersion in km s^{-1} , R is the spherical cloud radius in pc, and M_{vir} is the cloud virial mass in M_{\odot} . Implicit in this equation is the assumption that the virial parameter equals one.

Other works, in particular those focused on Milky Way clouds, have treated clouds as ellipsoids and used the corresponding form of the virial theorem (e.g. Bertoldi & McKee 1992), instead of the simplified Equation 7. Because of the low resolution and S/N of extragalactic observations, this approach is untenable. Under these conditions, deconvolution becomes very difficult and the precise shape of the source is hard, if not impossible, to recover. We note that the more complex measurements of cloud dimensions reduce to the Rosolowsky & Leroy (2006) RMS size parameter for use in the Bertoldi & McKee (1992) formulation of the virial theorem.

To relate the mass surface density, Σ_{GMC} , to the coefficient of the *size-line width* relation, $\sigma_v = C R^{0.5}$, we simply divide Equation 7 by the area of the cloud, πR^2 , to obtain

$$\Sigma_{GMC} = 331 C^2, \quad (8)$$

where the coefficient C is in units of $\text{km s}^{-1} \text{ pc}^{-0.5}$ and the surface density is expressed in $M_{\odot} \text{ pc}^{-2}$.

3.5. Estimate Uncertainties

The errors quoted in this paper are derived from bootstrapping the data in each cloud and re-deriving its properties. This yields a realistic assessment of the uncer-

tainty *once signal has been apportioned into clouds*. We also include a 25% gain uncertainty in the luminosity, typical of the uncertainty in the flux calibration at millimeter wavelengths. In high S/N cases, e.g. our N 83 and N 159 data sets, bootstrapping yields very low uncertainties. In these cases, virtually all of the uncertainty in the derived cloud properties rests with the apportionment of emission into clouds. This uncertainty is not included in our results.

4. RESULTS

4.1. Derived Cloud Properties

Table 3 presents our measurements of GMC properties in dwarf galaxies (available in full in the electronic edition). In order the columns list: (1) the galaxy that contains the GMC; (2) a number identifying the cloud; (3) the transition, CO $J = 2 \rightarrow 1$ or $1 \rightarrow 0$, being observed; (4) the right ascension and (5) declination of the intensity-weighted cloud center; (6) the mean LSR velocity of the cloud in km s^{-1} ; (7) the log of the cloud radius, in parsecs; (8) the log of the line of sight velocity dispersion of the cloud, in km s^{-1} ; (9) the log of the luminous mass from Equation 5; (10) the log of the virial mass from Equation 7; and (11) the peak brightness temperature in the cloud, in Kelvin. Uncertainties from bootstrapping are listed with each measurement.

Table 4 summarizes some of our results on a per galaxy basis. In order the columns list: (1) galaxy name; (2) number of measured GMC sizes in either CO transition; (3–4) average and range of GMC masses, in units of $10^5 M_\odot$; (5–6) error-weighted average and range of the logarithm of X_{CO} , in units of our adopted Galactic value; (7–8) error-weighted average and range of the coefficient of the *size-line width* relation, $\sigma_v R^{-0.5}$; and (9) corresponding average GMC surface density from Equation 8.

We checked for correlations between parameters in Table 4 and distance or resolution, and found none obvious. The major bias present, which is unavoidable, is that there is a correlation between our minimum virial mass and distance that is simply due to sensitivity. In that sense we sample different ranges of GMC mass in different galaxies. Considerations such as the nonlinearity of the *mass-luminosity* relation, for example, become important in the Magellanic Clouds where the cloud masses are small.

4.2. The Extragalactic Size-Line Width Relation

Of the three Larson relations perhaps the most fundamental one is that between cloud size and line width (Equation 1), as it is mostly (but not entirely) independent of the details of the excitation of the tracer molecule. The initial studies already pointed out the connection between the *size-line width* relation and expectations from the Kolmogorov theory for subsonic turbulence in incompressible fluids (Larson 1979, 1981). Later measurements in the inner Galaxy allowed a better determination of the relationship, showing that the exponent is not $1/3$ as it would be expected for a pure Kolmogorov cascade, but rather the steeper 0.5 ± 0.05 used in Equation 1 (Solomon et al. 1987). An index of 0.5 is consistent with expectations for compressible supersonic magnetohydrodynamic turbulence (also known

as Burger’s turbulence, Vestuto, Ostriker, & Stone 2003; Brunt & Mac Low 2004). Heyer & Brunt (2004) show that this relationship extends also within GMCs, which is consistent with the multi-scale turbulence interpretation of the observed line widths. The authors argue that because the *size-line width* relation is well-defined it implies the invariance and universality of the turbulent scaling relations. For clouds in virial equilibrium $M \sim R\sigma_v^2$, thus the observed *size-line width* relation implies $M \sim R^2$, or equivalently that all clouds have similar surface densities.

Recent studies of cloud properties in the outer Galaxy have shown that the *size-line width* relation breaks down for very small clouds. In these objects the velocity dispersion σ_v becomes a constant independent of their size (Heyer et al. 2001). These authors find that outer disk clouds smaller than ~ 7 pc in radius have an almost constant velocity dispersion $\sigma_v \sim 0.8 \text{ km s}^{-1}$, while clouds larger than ~ 7 pc follow the usual scaling. Heyer et al. interpret this fact in terms of the dynamical equilibrium state of the small clouds. These clouds have a virial parameter $\alpha = M_{\text{vir}}/M_{\text{lum}}$, representing their ratio of kinetic to gravitational energy, that is $\alpha \geq 1$ for masses below $M \sim 1.3 \times 10^4 M_\odot$. Thus these small clouds have an excess of kinetic energy over their self-gravity, are not in virial equilibrium, and in order to be bound they have to be confined by an external pressure of order $P/k \sim 10^4 \text{ cm}^{-3} \text{ K}$. The precise location of the break in the *size-line width* relation is then likely a function of the local pressure of the cloud environment. Similarly, analysis of the ^{13}CO emission from GMCs in the inner 3 kpc of the Milky Way reveals a less steep *size-line width* relation than that obtained from ^{12}CO studies, $\sigma_v \sim R^{0.15-0.30}$ (Simon et al. 2001). These authors conclude that although cloud complexes are bound, many of the clumps identified in their study are not gravitationally bound, probably due in part to the methodology of their clump identification algorithm. Finally, Oka et al. (2001) measured the GMC properties near the Galactic Center, finding that those clouds have line widths a factor of 3 to 5 times larger than similar clouds in the disk and suggesting that this is due to the large pressure in this region. These studies show that there are observed departures from the traditional *size-line width* relation in the Milky Way, in the direction of larger line widths for a given size.

Figure 1 shows our results for the ensemble of extragalactic clouds. Remarkably, dwarf galaxy cloud measurements are broadly compatible with the Milky Way *size-line width* relation, represented by the gray area and the small dots from the sample of Solomon et al. (1987). Detailed inspection of the data reveals, however, that there is a tendency for GMCs in dwarf galaxies to fall preferentially under the Galactic relationship. This is most apparent in a few clouds in the LMC, IC 10, and most clouds in the SMC, which are significantly inconsistent with the Milky Way. Note that these departures occur in the direction opposite from those described in the previous paragraph. While we may suspect that cloud measurements yielding sizes $R \gtrsim 100$ pc are affected by blending (such as those on the right side of the diagram), we have no reason to think that there are problems with the LMC, SMC, or IC 10, where we have some of the best spatial resolutions in the dataset. Furthermore, the

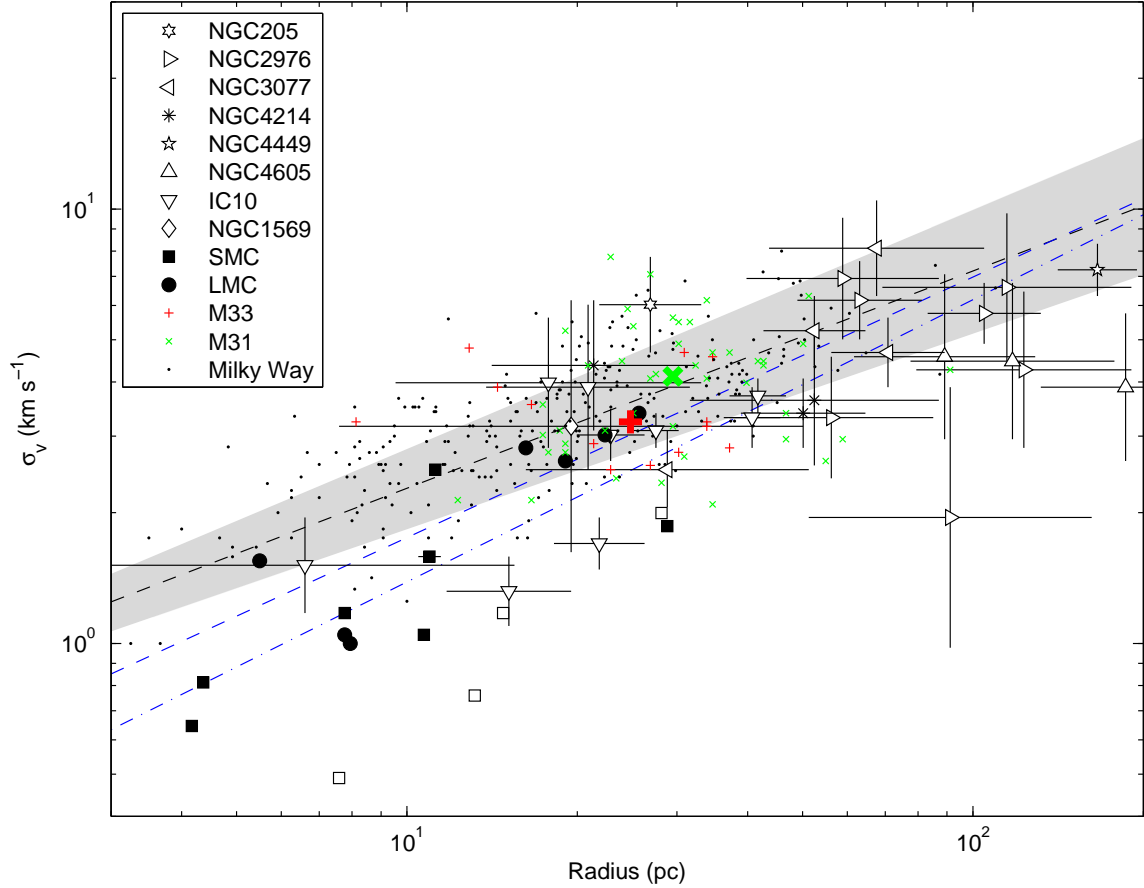


FIG. 1.— Extragalactic *size-line width* relation. The different symbols and the associated error bars indicate the measurements of molecular clouds in different galaxies. The black dots correspond to the sample of Milky Way clouds by Solomon et al. (1987). The open and filled symbols indicate measurements based on CO (1 – 0) and (2 – 1) observations respectively. The dashed black line and the gray area indicate the standard relationship for the Milky Way and its uncertainty, $\sigma_v = (0.72 \pm 0.07)R^{0.5 \pm 0.05}$. The dashed blue line illustrates the fit to the extragalactic GMC sample represented by Equation 9. The dash-dotted blue line indicates the fit to the dwarf galaxies only. The large color symbols indicate the median centroids for the GMCs in M 31 and M 33, our control sample. Dwarf galaxies are mostly compatible with the Galactic *size-line width* relation, with a tendency to deviate in the direction of smaller velocity dispersions for a given cloud size. In this regard the most discrepant points belong to the Small Magellanic Cloud and IC 10, some of the lowest metallicity galaxies in the sample. This is not, for the most part, a bias introduced by our methodology as the M 31 and M 33 points appear to follow the Galactic relationship.

control sample of M 31 and M 33 GMCs is entirely consistent with the Galactic *size-line width* relation and does not suffer from the same offsets. We discuss the particular situation of the SMC, which exhibits the most convincing departures, in §5.4. Note that Rubio et al. (1993b) arrived at a different conclusion in their study of the SMC. Because the GMC samples do not substantially overlap it is difficult to assess the source of the discrepancy. We attribute it mostly to the differences in the analysis methodologies, albeit it is possible that the samples are intrinsically different (perhaps due to different radiation environments).

Although it is not entirely correct to derive a unique *size-line width* relation for the ensemble of extragalactic data, we have determined a best fit relation. In order to avoid driving the result with the small formal error bars in the Magellanic Clouds, and to better represent the scatter in the data, we increase the errors in quadrature in both variables until we obtain a best fit χ^2 value of unity. The resulting relation, illustrated by the dashed blue line in Figure 1, is

$$\sigma_v \approx 0.44^{+0.18}_{-0.13} R^{0.60 \pm 0.10} \text{ km s}^{-1}, \quad (9)$$

where the data are fit in the log-log plane with simultaneous errors in both variables, and the error bars are derived using a bootstrapping technique. If we only use the dwarf galaxy data, the coefficient and the exponent are $0.31^{+0.09}_{-0.07}$ and 0.65 ± 0.07 respectively.

If the *size-line width* relation is interpreted in terms of virialized self-gravitating clouds supported mainly by turbulence, the compatibility between the Galactic relation and our measurements implies that most GMCs in dwarf galaxies have surface densities not very different from Galactic GMCs, for which $\Sigma_{\text{GMC}} \approx 170 \text{ M}_{\odot} \text{ pc}^{-2}$. Extragalactic GMCs that fall under the Galactic *size-line width* relation would have lower surface and volume densities than corresponding clouds in the Milky Way. The small-size, low velocity dispersion end of the dash-dotted line in Figure 1 corresponds to a drop of approximately a factor of 2 in the velocity dispersion, which translates to a factor of 4 decrease in surface density with respect to the Galactic value. This surface density may be ap-

appropriate for the most extreme galaxies in the sample (c.f., Table 4). If we fit a model that is proportional to $R^{0.5}$, the sample of dwarf galaxies is consistent with an average surface density $\Sigma_{\text{GMC}} \sim 85 \text{ M}_{\odot} \text{ pc}^{-2}$.

An alternative possibility is that the virial parameter, a measure of the ratio of kinetic to gravitational energy of the cloud (Bertoldi & McKee 1992), is different for these objects. The virial parameter, α , can be expressed in terms of the velocity dispersion following Equation 27 in McKee & Ostriker (2007) to obtain $\sigma_v = \sqrt{\alpha \Sigma_{\text{GMC}}} R^{-0.5}$. Thus, a low coefficient in the *size-line width* relation can be attributed to a lower than Galactic virial parameter. Bound clouds in the Milky Way have $\alpha \sim 1$, while pressure-confined clouds exhibit $\alpha \gg 1$ — a cloud in equilibrium with $\alpha < 1$ requires some additional type of support, presumably provided by magnetic fields. On the spatial scales studied here, such support is usually unimportant in the Milky Way.

4.3. The Luminosity-Line Width and Luminosity-Size relations

Figures 2 and 3 show the relations between ^{12}CO luminosities and either velocity dispersion or cloud radius. These luminosities can be related to the corresponding luminous mass M_{lum} for a Galactic X_{CO} using Eqs. 5 and 6. The steep dependency on σ_v in Equation 2 is a direct consequence of the observed *size-line width* relation in combination with the assumption of virial equilibrium. The coefficient in front of this equation reflects a combination of the area filling fraction by CO clumps within the resolved cloud, and the kinetic temperature of the gas itself.

Inspection of Figures 2 and 3 reveals that, despite the variety of environments sampled and the consistently lower-than-Galactic metallicity of our sources, there is good agreement between the properties of extragalactic and Galactic GMCs. Nonetheless, it is clear that there is an overall tendency for clouds in dwarf galaxies to be underluminous for their size, and clouds in the SMC tend to be also overluminous for their velocity dispersion. In other words, they tend to be larger and (in the case of the SMC) more quiescent (as traced by their velocity dispersion) than Milky Way GMCs of similar luminosity. The fit to all the extragalactic data, conducted as in §4.2, shows that the *luminosity-line width* relation is

$$L_{\text{CO}} \approx 645_{-132}^{+165} \sigma_v^{3.35 \pm 0.19} \text{ K km s}^{-1} \text{ pc}^2, \quad (10)$$

where the shallower-than-Galactic slope is driven mostly by the small SMC clouds. A similar analysis but including only the dwarf galaxy data yields a coefficient 688_{-167}^{+220} and an exponent 3.43 ± 0.22 , thus very consistent with the results when M 31 and M 33 are included. The corresponding extragalactic *luminosity-size* relation is

$$L_{\text{CO}} \approx 7.8_{-3.7}^{+6.9} R^{2.54 \pm 0.20} \text{ K km s}^{-1} \text{ pc}^2, \quad (11)$$

where the corresponding coefficient and exponent when fitting only the dwarf galaxy data are $6.0_{-2.3}^{+3.8}$ and 2.47 ± 0.17 . This shows that the data are completely consistent with the Galactic slope, but the relation is noticeably displaced toward lower luminosities for a given size.

Figure 3 suggests that, despite our efforts to correct for them, there may be a remaining methodological offset in the cloud size determination between the sample of Solomon et al. (1987) and this study, of order 30% toward larger R (equivalent to a factor of 0.5 toward lower luminosities). Unfortunately, establishing the origin of these offset would require a full reanalysis of the original Galactic survey. With the quality of the data at hand it is difficult to assert whether methodological or real offsets are driving the observed shift toward larger cloud sizes, although it seems that the likely methodological offsets are too small to explain the level of discrepancy in many sources — most notably the SMC.

Figure 4 illustrates the behavior of luminosity and virial mass described by equation 4 for our sample of extragalactic GMCs. Solomon et al. discuss this empirical relation in some detail, showing that it is a natural outcome of the combination of the *size-line width* relation with the assumption of virial equilibrium when all clouds share similar kinetic temperatures and area filling fractions in their resolved CO emission. Despite the aforementioned tendency for clouds in dwarf galaxies to be underluminous for their sizes, their virial masses are, on average, only slightly underpredicted by their CO luminosity. In the particular case of GMCs in the SMC, because the observed departures from the standard *luminosity-line width* and *luminosity-size* relations occur in opposite directions, their larger sizes and smaller velocity dispersions for a given luminosity approximately cancel out in the virial mass calculation. Thus most reliable extragalactic clouds in our sample are remarkably compatible with equation 4. The fit to the entire extragalactic sample yields

$$M_{\text{vir}} \approx 7.6_{-2.6}^{+3.9} L_{\text{CO}}^{1.00 \pm 0.04} \text{ M}_{\odot}, \quad (12)$$

while the fit to the dwarf galaxies only has a coefficient of $10.3_{-3.7}^{+5.8}$, and an exponent 1.00 ± 0.05 . Thus the extragalactic and Galactic *mass-luminosity* relations are in excellent agreement for GMCs in the mass range $10^3 - 10^5 \text{ M}_{\odot}$. This suggests that, by comparison with Equation 6, X_{CO} is on average a factor of 1.7 to 2.3 larger than our adopted Galactic value of $2 \times 10^{20} \text{ cm}^{-2} (\text{K km s}^{-1})^{-1}$ (although with large error bars). We will discuss the consequences for X_{CO} and the presence of any metallicity trends in the CO-to- H_2 conversion factor in §5.2.

4.4. Comparison with Complete Samples

We outlined in §1.1 some of the conclusions of the recent study of the Local Group by Blitz et al. (2007). We employed here the same datasets for M 31 and M 33, analyzing them with a later version of the same CPROPS algorithm. While Blitz et al. emphasized completion to study the cloud statistics, the present analysis made use of the available data with the best possible combination of sensitivity and resolution, thus employing different datasets for the Magellanic Clouds and IC 10. Furthermore, this study incorporates a large number of galaxies in and beyond the Local Group that were not analyzed in Blitz et al. (2007). Many of the results, however, are reassuringly similar: extragalactic GMCs broadly share the same properties observed in Milky Way GMCs, although the clouds in some galaxies (notably the SMC) appear to be somewhat different from the remainder of

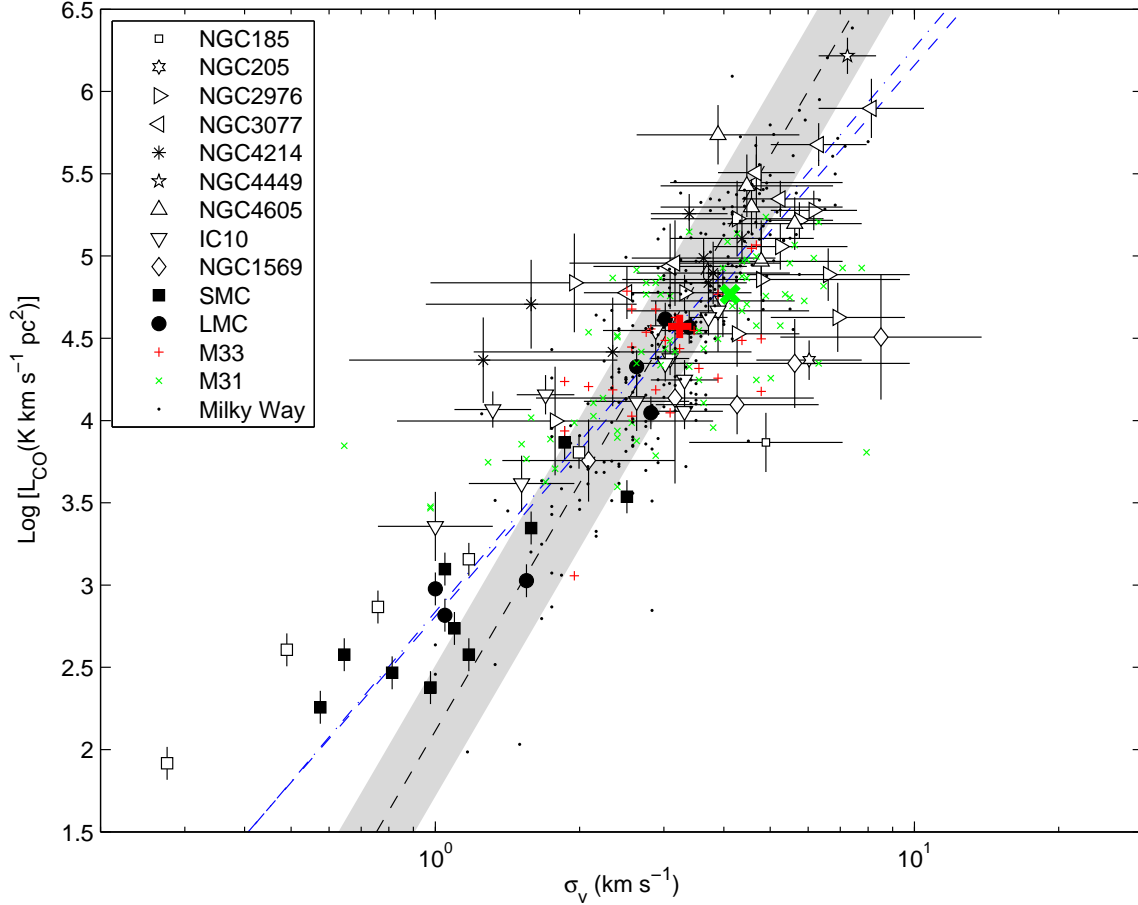


FIG. 2.— Extragalactic *luminosity-line width* relation. As in Fig. 1, the different symbols and the associated error bars indicate the measurements of molecular clouds in different galaxies, with open and filled symbols indicating measurements based on CO (1 – 0) and (2 – 1) observations respectively. The black dots correspond to the sample of Milky Way GMCs by Solomon et al. (1987), and the gray regions to their 1σ dispersion around the dashed lines, which follow Equations 2 and 3. The dashed blue line illustrates the fits to the extragalactic GMCs. The dash-dotted blue line corresponds to the results of the fits for the dwarf galaxy data only. The large color symbols indicate the median centroids of the clouds that have R measurements for our control sample of GMCs in M 31 and M 33.

the sample. We will argue later (§5.4) that this is probably caused by the low metallicity of the parent galaxy.

5. DISCUSSION

5.1. Implications for Photoionization-Regulated Star Formation

McKee (1989) discusses a self-regulated theory of star formation, where photoionization caused by the interstellar radiation field controls the rate at which clouds contract and form new stars. In this theory clouds undergo contraction until the energy input by the newly formed stars balances the gravitational collapse. Support against contraction at the level of individual clumps is provided by their magnetic field. This contraction happens at the ambipolar diffusion rate, as the neutrals diffuse through the ions which are anchored by the magnetic field. The rate of diffusion is determined by the ionization fraction of the cloud, which in its outer regions (which comprise most of its mass) is set by the ultraviolet interstellar radiation field (ISRF), and in its inner regions is due to cosmic ray ionization. The total rate of star formation of a cloud thus depends critically on its extinction and radiation environment. Clumps immersed

in weaker ISRFs require less extinction to collapse, and vice versa.

These ideas have considerable implications for the structure of GMCs as a function of environment, and it is of great interest to test their predictions. In the theory outlined by McKee (1989), extinction is the key parameter that regulates the equilibrium of clouds, not total column density. Accordingly, McKee proposed as one of the key tests of the theory that clouds in galaxies with different metallicities and dust-to-gas ratios should obey different *size-line width* relations, as

$$\sigma_v \approx 0.72 \left(\frac{\bar{A}_V}{7.5\delta_{gr}} \right)^{0.5} R^{0.5} \text{ km s}^{-1}. \quad (13)$$

This expression is the analog of equation 1, where the numerical coefficient now incorporates the cloud mean extinction, \bar{A}_V , and the ratio of A_V extinction per hydrogen nucleus relative to the Milky Way, δ_{gr} , so that for Galactic clouds we recover the standard *size-line width* relation. The prediction from photoionization-regulated star formation theory is that equilibrium molecular clouds in galaxies with low values of δ_{gr} should have

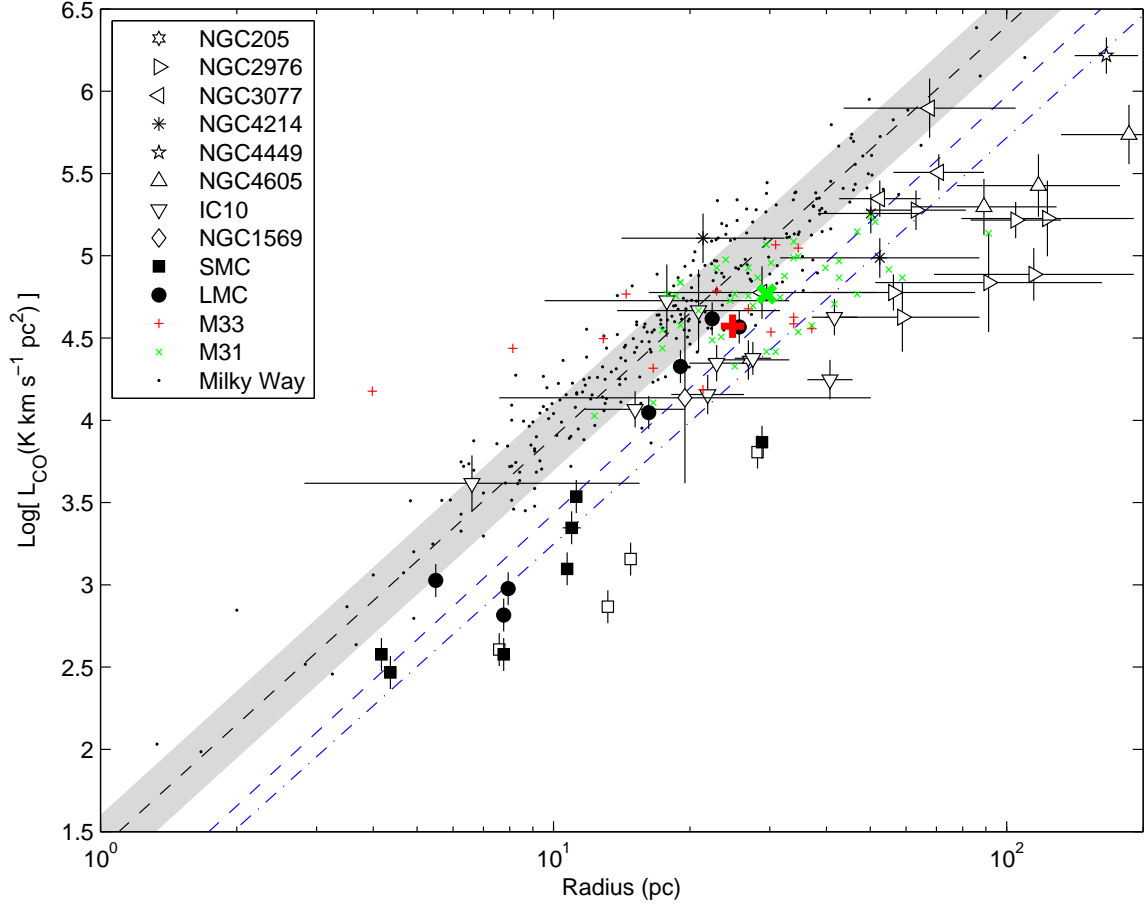


FIG. 3.— Extragalactic *luminosity-size* relation. Symbols and labels as in Fig. 2.

TABLE 3
RADIO OBSERVATIONS

Galaxy	#	Trans.	R.A. (J2000)	Declination (J2000)	V_{LSR} (km s ⁻¹)	$\log_{10} R$ (pc)	$\log_{10} \sigma$ (km s ⁻¹)	$\log_{10} M_{\text{lum}}$ (M _⊙)	$\log_{10} M_{\text{vir}}$ (M _⊙)	T_B (K)
BIMA										
NGC185	1	1 → 0	00 ^h 38 ^m 56.4 ^s	48°20′19.9″	-194.1	...	0.69 ± 0.16	4.52 ± 0.18	...	1.2
NGC205	1	1 → 0	00 ^h 40 ^m 24.0 ^s	41°41′52.1″	-248.9	1.43 ± 0.09	0.78 ± 0.11	5.02 ± 0.12	6.01 ± 0.24	1.0
NGC2976	1	1 → 0	09 ^h 47 ^m 23.6 ^s	67°54′40.1″	-31.3	1.77 ± 0.17	0.84 ± 0.14	5.28 ± 0.21	6.46 ± 0.30	0.3
NGC2976	2	1 → 0	09 ^h 47 ^m 24.1 ^s	67°54′33.9″	-24.8	...	0.25 ± 0.33	4.65 ± 0.33	...	0.3
NGC2976	3	1 → 0	09 ^h 47 ^m 14.9 ^s	67°54′44.0″	-19.5	1.75 ± 0.18	0.52 ± 0.14	5.43 ± 0.11	5.82 ± 0.30	0.4
NGC2976	4	1 → 0	09 ^h 47 ^m 18.4 ^s	67°54′48.5″	-6.2	2.06 ± 0.22	0.82 ± 0.17	5.54 ± 0.16	6.71 ± 0.28	0.3
NGC2976	5	1 → 0	09 ^h 47 ^m 17.3 ^s	67°54′59.2″	5.5	1.96 ± 0.25	0.29 ± 0.30	5.49 ± 0.30	5.56 ± 0.51	0.3
NGC2976	6	1 → 0	09 ^h 47 ^m 15.3 ^s	67°55′04.9″	15.4	2.09 ± 0.19	0.63 ± 0.18	5.88 ± 0.23	6.37 ± 0.28	0.4
NGC2976	7	1 → 0	09 ^h 47 ^m 15.3 ^s	67°55′16.7″	20.8	...	0.68 ± 0.29	5.51 ± 0.36	...	0.3
NGC2976	8	1 → 0	09 ^h 47 ^m 13.0 ^s	67°54′54.5″	-2.6	...	0.63 ± 0.13	5.18 ± 0.20	...	0.3

NOTE. — Table 3 is published in its entirety in the electronic edition of the *Astrophysical Journal*. A portion is shown here for guidance regarding its form and content.

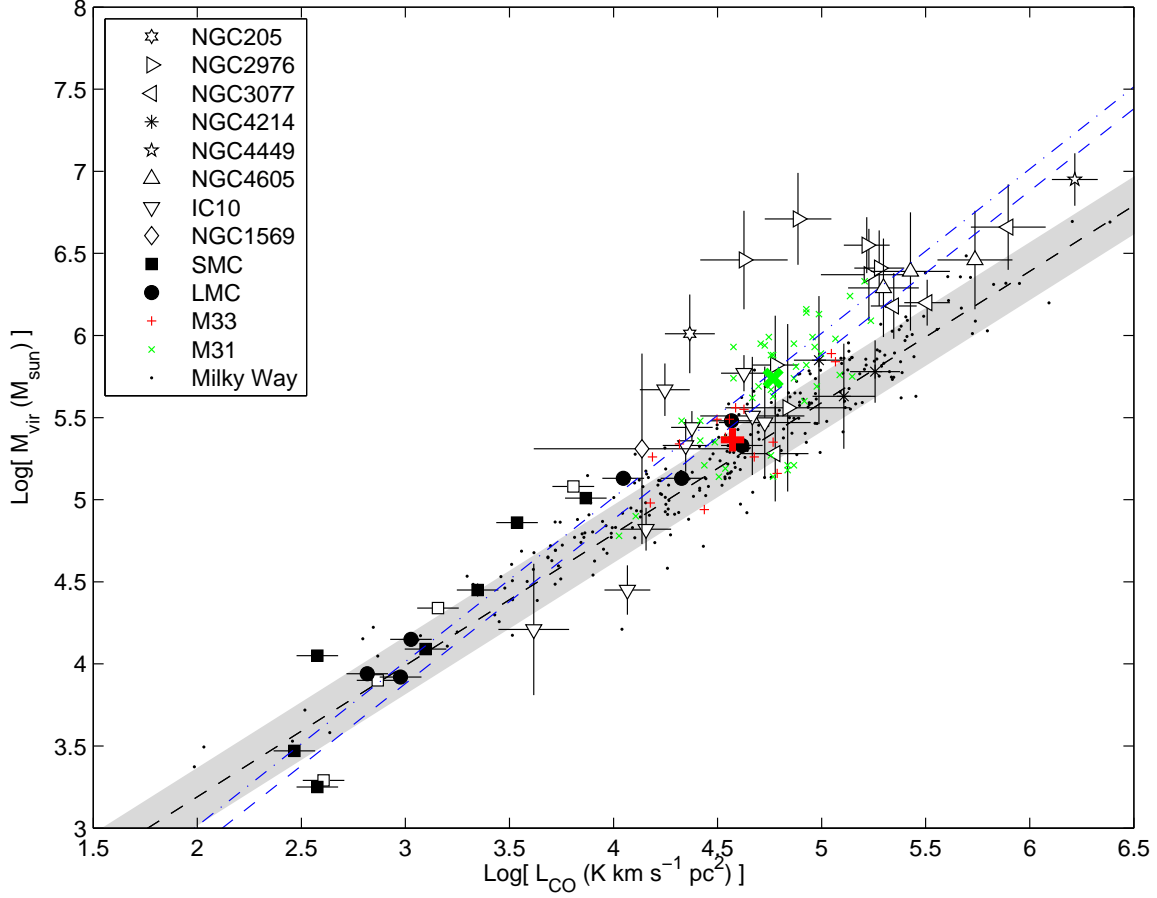


FIG. 4.— The relationship between CO luminosity, L_{CO} , and virial mass, M_{vir} , for Galactic and extragalactic GMCs. As in previous figures white and black symbols indicate measurements based on CO 1 – 0 and 2 – 1 respectively. The dots correspond to the sample of Milky Way GMCs by Solomon et al. (1987). The dashed black line illustrates equation 4, with the gray region corresponding to the Galactic 1σ dispersion around the line ($\approx 50\%$). The dashed and dash-dotted blue lines illustrate the fits for all extragalactic GMCs and for the dwarf galaxy sample alone, respectively.

TABLE 4
GALAXY-WIDE MEASURED GMC PROPERTIES

Galaxy	Meas.	$M_{\text{vir}}/10^5$ (M_{\odot})		$\log [X_{\text{CO}}/2 \times 10^{20}]$ ($\text{cm}^{-2}(\text{K km s}^{-1})^{-1}$)		$\sigma_v R^{-0.5}$ ($\text{km s}^{-1} \text{pc}^{-0.5}$)		Σ_{GMC} ($M_{\odot} \text{pc}^{-2}$)
		mean	range	mean ¹	range ²	mean ¹	range	
IC 10	9	2.6	0.2 – 5.6	$+0.28 \pm 0.07$	0.5 – 5.9	0.57 ± 0.08	0.34 – 0.94	108 ± 31
NGC 205	1	10.4	...	$+0.99 \pm 0.27$...	1.16 ± 0.25	...	447 ± 191
SMC	11	0.1	0.02 – 1.2	$+0.43 \pm 0.03$	1.1 – 6.6	0.37 ± 0.08	0.18 – 0.75	45 ± 21
LMC	7	1.3	0.1 – 3.1	$+0.30 \pm 0.04$	1.1 – 3.0	0.61 ± 0.10	0.35 – 0.70	123 ± 39
NGC 1569	1	2.1	...	$+0.52 \pm 0.78$...	0.72 ± 0.44	...	170 ± 209
NGC 2976	7	26.4	3.6 – 53	$+0.67 \pm 0.11$	1.2 – 15.1	0.57 ± 0.06	0.20 – 0.90	106 ± 21
NGC 3077	4	16.0	1.9 – 48	$+0.06 \pm 0.12$	0.7 – 1.5	0.71 ± 0.08	0.47 – 0.99	166 ± 39
NGC 4214	3	6.0	4.3 – 6.9	-0.07 ± 0.17	0.7 – 1.6	0.56 ± 0.12	0.48 – 0.94	102 ± 44
NGC 4449	1	85.3	...	$+0.08 \pm 0.19$...	0.56 ± 0.09	...	105 ± 33
NGC 4605	3	24.2	19 – 30	$+0.23 \pm 0.21$	1.2 – 2.2	0.37 ± 0.08	0.29 – 0.48	44 ± 18
M 31	44	5.3	0.6 – 21	$+0.26 \pm 0.03$	0.5 – 5.0	0.72 ± 0.03	0.35 – 1.62	172 ± 15
M 33	14	2.3	0.9 – 8.0	$+0.12 \pm 0.06$	0.5 – 2.6	0.70 ± 0.07	0.46 – 2.40	160 ± 31

¹ Error-weighted mean and corresponding error.

² Range for $X_{\text{CO}}/2 \times 10^{20}$.

high velocity dispersions for a given size. In other words, clouds in low metallicity environments need to be more massive to attain the characteristic extinction in their inner regions for a given ISRF.

Figure 5 shows the average coefficient of the *size-line width* relation for each galaxy in our sample plotted as a function of metallicity, which is a good proxy for δ_{gr} in equation 13. Neither the placement of individual GMCs in the *size-line width* relation (Fig. 1), nor Fig. 5 show evidence of the systematic behavior predicted by the theory. If anything, clouds in IC 10 ($\delta_{gr} \sim 0.3$) and the SMC ($\delta_{gr} \lesssim 0.2$), which should have higher-than-Galactic velocity dispersions by factors of $\sim 2 - 3$, appear to have systematically lower-than-Galactic values of velocity dispersion for a given size. Even if we discard the clouds that fall under the Galactic *size-line width* relation as potentially out of equilibrium or perhaps magnetically supported, the remaining clouds do not show larger than Galactic velocity dispersion. It is important to realize that several of these GMCs exist in environments of larger-than-Galactic ISRF (e.g., Israel et al. 1996), so that the observed lack of a trend in $\sigma_v R^{-0.5}$ is not directly caused by a cancellation between the effects of ISRF and metallicity.

Early support for photoionization regulated star formation was found by Pak et al. (1998), who used IRAS 60 and 100 μm data, a model of PDR regions, and H_2 and [CII] measurements to derive the structure of molecular clouds in the Magellanic Clouds. Their determination of column densities, however, hinges critically on the estimate of the radiation field, which is derived from IRAS measurements. In the SMC they model dust temperatures in the range of 42 – 49 K, higher than the temperatures in the Stanimirović et al. (2000) map which employs the same data. We use the IRIS data to check the temperature towards LIRS36, one of their target regions, and find it to be 33 K instead of the 45 K derived by Pak et al. (1998). Because the estimated radiation field is very strongly dependent on the assumed dust temperature, this alone suggests a ~ 5 times lower field than they adopt. This is enough to bring their result into approximate agreement with our own, and makes the radiation field in this region intermediate between Galactic and 30 Doradus in the LMC. A further concern with this analysis stems from the use of 60 μm data to establish a temperature, as it is known that there is an important contribution from stochastically heated small grains at this wavelength (particularly in the Magellanic Clouds, Bernard et al. 2008). Studies combining 100 μm data with 160 – 170 μm (Leroy et al. 2007; Wilke et al. 2004) determine typical temperatures of 20 – 23 K for these SMC regions.

While our analysis does not directly support photoionization-regulated star formation theory, there are several caveats that need to be considered before rejecting it. First, strictly speaking the increased column density prediction from photoionization-regulated star formation theory applies to the structures that form stars. Thus, it is possible that these observations do not sample the scales at which the column density enhancements occur. Second, in addition to assuming clouds in virial equilibrium, this prediction assumes that the ratio of mean clump to cloud extinction is similar to Galactic

clouds, and that the characteristic density (at which cosmic ray ionization is $\approx 10^{-7}$) is a similar fraction of the cloud density as in Galactic clouds. Unfortunately, these parameters are almost completely unconstrained for extragalactic GMCs. Third, metallicity may not be a good linear proxy for δ_{gr} . This parameter folds in the effects of dust-to-gas ratio and extinction, and although dust-to-gas ratio likely tracks metallicity the dependence of extinction on metallicity may be important. In the SMC $N(\text{H I})/A_V \approx 13.2 \times 10^{21} \text{ cm}^{-2} \text{ mag}^{-1}$, a factor of 6.5 larger than McKee’s adopted Galactic value and compatible with the ratio of metallicities between the SMC and the Milky Way (Gordon et al. 2003). At ultraviolet wavelengths, however, Gordon et al. find that A_λ/A_V is larger than Galactic by factors of 2–3. As a result of this, and assuming that the ultraviolet extinction and not A_V is the parameter that matters at setting the cloud ionization level, we may probe a smaller range of δ_{gr} than that assumed in Fig. 5. Note that although this consideration diminishes the discrepancy with the theoretical predictions it does not eliminate it. Fourth, equation 13 requires that CO is present throughout the molecular material so that its velocity dispersion accurately samples the potential of the GMC. This may not be the case in low metallicity environments if there are large H_2 envelopes faint in CO surrounding the CO-bright portions of the GMC, and it may constitute the biggest limitation in our test of photoionization-regulated star formation. Nonetheless, the result stands that there is no observed trend of increasing velocity dispersion in the *size-line width* relation for decreasing metallicity on the scales sampled — *clouds show strikingly similar properties in all galaxies.*

5.2. The CO-to- H_2 Conversion Factor

5.2.1. Background

Using ^{12}CO observations to measure the amount of molecular hydrogen requires assuming a CO-to- H_2 conversion factor $X_{\text{CO}} = N(\text{H}_2)/\int I(\text{CO}) dv$ (Lebrun et al. 1983). This factor incorporates the effects of abundance, excitation, and cloud structure averaged over a large area. The optically thick ^{12}CO 1 – 0 transition can be used to trace the molecular mass of a cloud because it arises from the surfaces of clump ensembles within the telescope beam: by measuring I_{CO} we are counting clumps, and under very general conditions the CO intensity will be proportional to the total molecular mass of the clump ensemble. This is the essence of the CO “mist” model discussed by Dickman et al. (1986). Because encompassing all the relevant physics of the problem into ab initio calculations is extremely difficult and not well constrained, astronomers rely on empirical calibrations of X_{CO} obtained using a variety of techniques (e.g., Dickman 1978; Sanders et al. 1984; Bloemen et al. 1986; Strong & Mattox 1996; Dame et al. 2001).

It is reasonable to expect that X_{CO} will depend on the local properties of the interstellar medium (ISM); volume density, temperature, radiation field, and metallicity (e.g., Kutner & Leung 1985; Elmegreen 1989; Bell et al. 2006). Observations throughout the Galactic disk, however, constrain X_{CO} within a narrow range $X_{\text{CO}} \approx (1.8 \pm 0.3) \times 10^{20} \text{ cm}^{-2} (\text{K km s}^{-1})^{-1}$, with excursions of up to a factor of ~ 2 over this value, particularly at

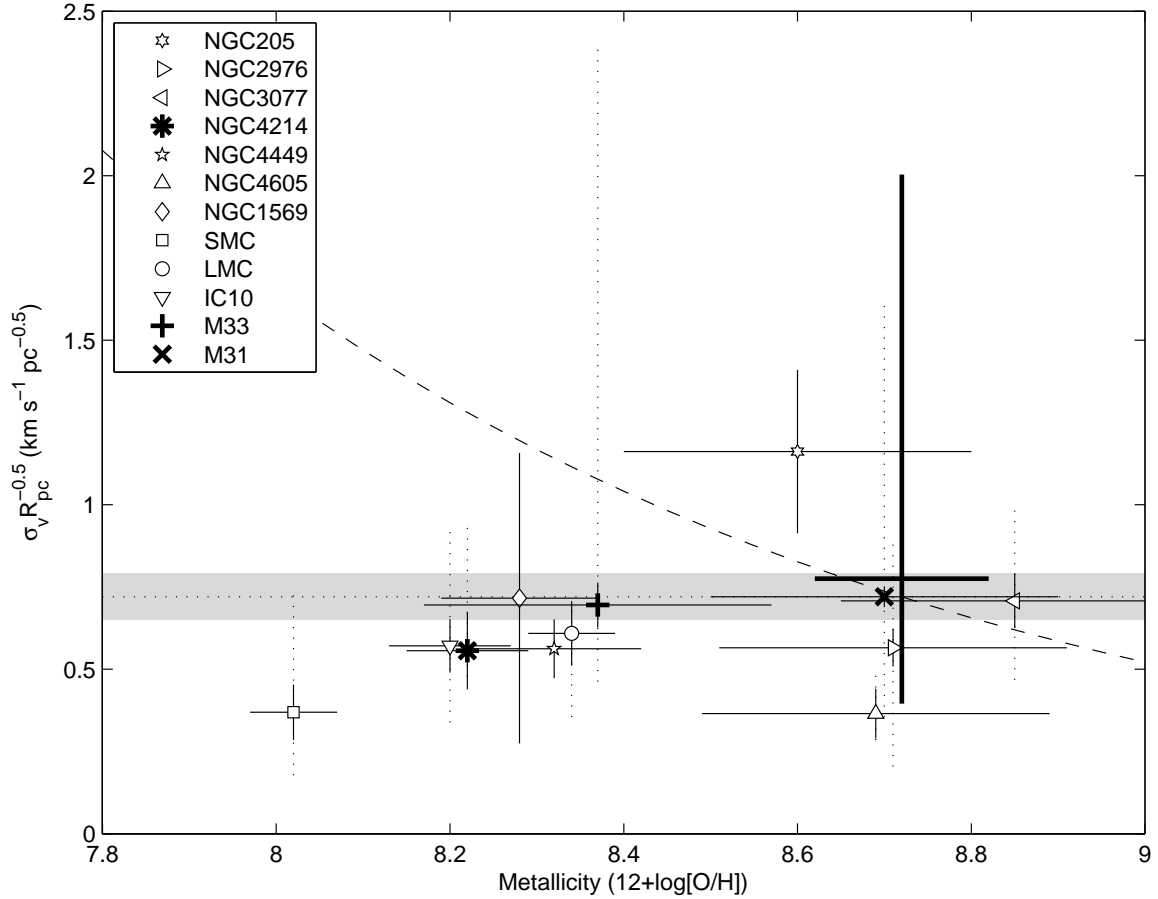


FIG. 5.— Coefficient of the *size-line width* relation for the different galaxies in our sample, as a function of metallicity. Each symbol represents the error-weighted average value of $\sigma_v/R^{0.5}$ for all clouds in a galaxy. The horizontal bars indicate the uncertainty in galaxy metallicity, while the vertical fill bar correspond to the error in the error-weighted average and the dotted vertical line illustrate the full range of values for $\sigma_v/R^{0.5}$ for individual clouds within a galaxy. The thick lines indicate the behavior for the Galactic sample of Solomon et al. (1987) corrected as described in the text, with the full range shown. The dashed line shows the expectation from equation 13 assuming that the normalized extinction per hydrogen nucleus (δ_{gr}) is proportional to the source metallicity, while the dotted horizontal line and gray area show the value of canonical Galactic coefficient in Equation 1, $0.72 \pm 0.07 \text{ km s}^{-1} \text{pc}^{-0.5}$. The fact that the dwarf galaxy points cluster under the Galactic value is just another manifestation of their tendency to fall under the Milky Way *size-line width* relation, discussed in §4.2.

high latitudes (Dame et al. 2001). This suggests that the local variations due to volume density, temperature, and radiation field are unimportant when cloud properties are averaged over a large area, which is the case for most extragalactic observations. In cases where the average conditions are very different from those in the Galaxy, however, differences in X_{CO} become apparent. For example, mass estimates of molecular clouds subjected to extreme radiation fields, such as those in starburst environments, suggest that they have an X_{CO} conversion factor 4 to 20 times smaller than in the Galaxy (e.g., Yao et al. 2003). This can be understood in terms of a larger emissivity per CO molecule in starburst galaxies, stemming from a higher excitation state due to larger physical temperatures and volume densities in these environments (e.g., Weiß et al. 2001). Another possibility is that a key assumption underlying the CO-to- H_2 proportionality, that the CO line width traces the H_2 mass, breaks down in very CO-rich systems (Downes et al. 1993). Similarly, X_{CO} conversion factors a few times lower than that of the Galactic disk are commonly observed in the centers of spiral galaxies, including our own (Sodroski et al. 1995;

Israel, Tilanus, & Baas 2006).

A property of the ISM that is expected to have a dramatic impact on the value of X_{CO} is its heavy-element abundance (Israel et al. 1986; Maloney & Black 1988). Unlike density or radiation field fluctuations, metallicity does not average out over the large areas sampled by a telescope beam. In fact, dwarf galaxies, which tend to have subsolar metallicities, show little evidence for metallicity gradients at least in the examples where such gradients could be well measured (e.g., Dufour 1984; Kobulnicky & Skillman 1997; Skillman 2003). Metallicity affects cloud structure in two ways: 1) directly, as smaller abundances of C and O translate into lower CO yields, and 2) indirectly, as the dust-to-gas ratio is lowered, which in turn diminishes the H_2 formation rates and the shielding of molecular gas from the photodissociating effects of ultraviolet radiation.

The observational effects expected from these changes can be summarized as follows: as metallicity decreases, decreasing dust shielding pushes the C^+ to CO transition further into the molecular gas. In terms of a spherical clump, the radius of the $\tau = 1$ surface for CO becomes

smaller as the metallicity decreases. Because at high-enough extinction most of the carbon in the gas phase turns into ^{12}CO , which in turn becomes rapidly optically thick, the actual C/H ratio of the gas has only a small effect on the position of $\tau = 1$ surface. For a typical Galactic cloud, for example, the C^+/CO transition occurs at $A_V \sim 2$ while the $\tau = 1$ surface of CO occurs at column densities $N_{\text{CO}} \sim 8 \times 10^{15} \text{ cm}^{-2} (\text{km s}^{-1})^{-1}$ which translate into visual extinction of $A_V \sim 0.015$ for a typical gas-phase carbon abundance. Thus, almost immediately after becoming the dominant form of carbon, ^{12}CO turns optically thick. Because of its large abundance, H_2 is self-shielding in Milky Way molecular clouds (Abgrall et al. 1992; Draine & Bertoldi 1996). CO, however, is only mildly self-shielding, although it also cross-shields with H_2 at column densities $N(\text{H}_2) \gtrsim 10^{21} \text{ cm}^{-2}$ (van Dishoeck & Black 1988). If the conditions are such that H_2 self-shielding dominates over dust shielding at lower metallicities, the atomic to molecular H I/ H_2 transition will not move into the cloud for decreasing dust-to-gas ratios. As a result, a molecular clump will not change its size with decreasing metallicity but its ^{12}CO emitting core will diminish, yielding an increasing X_{CO} conversion factor (e.g., Maloney & Black 1988; Bolatto, Jackson, & Ingalls 1999; Röllig et al. 2006).

5.2.2. Existing Calibrations

There are several observational calibrations of X_{CO} with metallicity, Z , in the literature, showing a range of behaviors. Most of the calibrations find an increasing X_{CO} with decreasing Z although the rate of increase varies greatly depending on the technique and the spatial resolution of the observations used.

A key datum in these calibrations is the measurement in the Small Magellanic Cloud, as this is the galaxy with the lowest metallicity where CO is reliably detected ($Z_{\text{SMC}} \approx 0.2Z_{\odot}$; Dufour 1984; Vermeij & van der Hulst 2002). In the first systematic study of this galaxy, Rubio et al. (1993b) used single-dish CO observations and the assumption of clouds in virial equilibrium to determine that $X_{\text{CO}} \sim 60 \times 10^{20} \text{ cm}^{-2} (\text{K km s}^{-1})^{-1}$ at a resolution of ~ 160 pc, while finding $X_{\text{CO}} \sim 9 \times 10^{20} \text{ cm}^{-2} (\text{K km s}^{-1})^{-1}$ on scales of ~ 15 pc. Mizuno et al. (2001) revisited the estimate of X_{CO} in the SMC with new single-dish observations at a resolution of ~ 50 pc and found $X_{\text{CO}} \sim 10 - 50 \times 10^{20} \text{ cm}^{-2} (\text{K km s}^{-1})^{-1}$, in rough agreement with the previous results. One important issue with these determinations is that it is unclear whether the large scale structures observed in CO are self-gravitating, virialized molecular clouds. The applicability of the virial theorem on scales of 100 pc and larger and the ability to accurately measure the size of the CO structures, both necessary to apply equation 7, are problematic. Another issue with these determinations is that they do not account for the finite angular resolution of the telescope, which is in many cases comparable to the sizes of the clouds. This will systematically bias these measurements in the direction of larger virial masses and larger X_{CO} .

Subsequently Rubio et al. (2004) used millimeter-wave continuum observations to obtain the mass of the quiescent cloud SMCB1-1 and compare it with its CO emission, reaching the conclusion that the dust-derived mass is 7 to 20 times larger than the cloud virial mass. They

suggest that this H_2 is located in an envelope of the cloud that does not emit brightly in CO. Very recently, Leroy et al. (2007) used new far-infrared (FIR) images of the SMC obtained by the *Spitzer* Space Telescope to model the dust emission and locally calibrate its dust-to-gas ratio, obtaining a map of H_2 in this galaxy. Comparison with the CO emission indicates that the H_2 clouds are on average $\sim 30\%$ more extended than the CO-emitting regions, so that CO clouds are immersed in an extended molecular envelope of H_2 . Furthermore, over the volume occupied by CO, Leroy et al. find $X_{\text{CO}} \sim 60 \times 10^{20} \text{ cm}^{-2} (\text{K km s}^{-1})^{-1}$, while the overall X_{CO} for the entire SMC is approximately twice that.

Among the calibrations for X_{CO} with metallicity, a number of them rely on the assumption of virial equilibrium to obtain the molecular mass of GMCs. Wilson (1995) used interferometric CO observations of M 33 and dwarf galaxies in conjunction with the aforementioned Rubio et al. (1993b) results to establish that $X_{\text{CO}} \sim Z^{-0.67}$, where Z is measured using the oxygen abundance, as O/H. Arimoto et al. (1996) used several observations in the literature to determine that $X_{\text{CO}} \sim Z^{-1}$. Employing some of the same interferometric observations analyzed here, Walter et al. (2001) determined a Galactic value for X_{CO} in NGC 4214, a galaxy where $Z \sim 0.3Z_{\odot}$. A result of 60% of the Galactic value was obtained in NGC 3077 (Walter et al. 2002), a galaxy with approximately Galactic metallicity. Similarly, Rosolowsky et al. (2003) used interferometric observations of the entire disk of M 33 and found no dependence of X_{CO} on metallicity over a range of 0.8 dex in Z (a factor of 6). All these studies are based on virial mass techniques.

Calibrations tend to be even more discrepant when other methods are employed. Besides the aforementioned results by Leroy et al. (2007), Israel (1997) used H I and Infrared Astronomy Satellite (IRAS) observations of several galaxies, estimating $X_{\text{CO}} \sim 120 \times 10^{20} \text{ cm}^{-2} (\text{K km s}^{-1})^{-1}$ in the SMC and finding a metallicity dependence $X_{\text{CO}} \sim Z^{-2.7}$, or $X_{\text{CO}} \sim Z^{-3.5}$ when taking into account the local interstellar radiation field. Madden et al. (1997) used measurements of the FIR [C II] ($^2\text{P}_{3/2} \rightarrow ^2\text{P}_{1/2}$) transition to estimate $X_{\text{CO}} \sim 50 \times 10^{20}$ in some regions of the low metallicity dwarf galaxy IC 10, and over 100 times the Galactic value overall ($Z_{\text{IC10}} \sim 0.3Z_{\odot}$). Imara & Blitz (2007) used stellar extinction in the LMC to measure $X_{\text{CO}} \sim 9.3 \times 10^{20} \text{ cm}^{-2} (\text{K km s}^{-1})^{-1}$, toward the low end of virial mass estimates for this source. Finally, Boselli, Lequeux, & Gavazzi (2002) found a milder $X_{\text{CO}} \sim Z^{-1}$ dependence using a combination of virial and dust-continuum methods. In summary, there are large discrepancies between the different authors and techniques, and in general estimates based on FIR observations find stronger dependencies on metallicity than those based on virial arguments, although typically they also probe larger scales.

A problem with the available studies has been the lack of uniformity in the datasets, methods, and analysis techniques. Unexpectedly, the most uniform calibration in the literature (that of Rosolowsky et al. 2003), where all the clouds are at the same distance, the spatial resolution is good (20 pc), and identical analysis is applied to the

data finds that X_{CO} is independent of Z . Very recent observations, however, cast doubts on the magnitude of the metallicity gradient in this galaxy. Rosolowsky & Simon (2007) find that the metallicity gradient of M 33 is a factor of 3 shallower than previously accepted, which implies that the Rosolowsky et al. (2003) GMC data probes a considerably smaller range of Z than previously thought. Thus mild metallicity dependencies of X_{CO} within this galaxy may be masked by the internal scatter of the measurements. Another potential issue is that similar gradients in the radiation field and metallicity with galactocentric distance have opposite effects and may conspire to produce an almost constant X_{CO} (Elmegreen 1989).

5.2.3. Our Results

The fact that the overwhelming majority of our extragalactic GMCs with reliable property determinations are compatible with the empirical Galactic relationship between L_{CO} and M_{vir} described by equation 4 (§4.3) implies that we do not observe extreme departures from a Galactic X_{CO} . Indeed, Figure 6 shows our results for the extragalactic calibration of X_{CO} with metallicity, using virial GMC masses. The gray region illustrates the approximate range of X_{CO} in the Milky Way found by Dame et al. (2001), a factor of 2 around the nominal $2 \times 10^{20} \text{ cm}^{-2} (\text{K km s}^{-1})^{-1}$. The thick lines show the dispersion of values for the GMCs in the Solomon et al. (1987) sample with masses larger than $10^5 M_{\odot}$. The symbols show the average of $M_{\text{vir}}/M_{\text{lum}}$ for all GMCs in each galaxy in our sample, with the corresponding vertical bars indicating the error and range of $M_{\text{vir}}/M_{\text{lum}}$ within a galaxy. The galaxy that shows the largest departure from Galactic X_{CO} is NGC 205, but with only one identified cloud we lack significant statistics. The situation is similar for NGC 1569. Note that although the GMCs in the SMC show an average X_{CO} three times Galactic, they are not unusual compared with Galactic clouds of the same mass (recall that Equation 4 is not a linear relation, and Galactic clouds with masses similar to our SMC clouds have similar ratios of virial to luminous mass; c.f., Figure 4). Thus, GMCs in dwarf galaxies are remarkably compatible with a Galactic X_{CO} independent of their metallicity, and any metallicity trends appear to be much weaker than the dispersion of the measurements.

To further quantify this statement we have carried out a number of fits to the data. We do not consider in the fits NGC 2976 (because of its uncertain metallicity), and the Milky Way (which may suffer from a systematic methodological offset). A least-squares bivariate fit $\log X_{\text{CO}} = a + b \log(O/H)$ with simultaneous errors in both axes to the measurements for all remaining galaxies yields a slope $b = -0.45 \pm 0.30$ and $\chi^2 \approx 21$, with errors estimated using bootstrapping. Increasing all errors proportionally to obtain $\chi^2 \approx 1$ yields $b = -0.23 \pm 0.25$. Similar fits to the data for the galaxies with the largest number of GMC measurements (M 31, M 33, IC 10, LMC, and SMC) yield $b = -0.46 \pm 0.30$ ($\chi^2 \approx 5$) and $b = -0.24 \pm 0.26$ ($\chi^2 \approx 1$). These results, plus the considerations in the paragraph above, confirm that there is no measurable trend in the resolved X_{CO} with metallicity present in the data. As we discuss below, however, this does not imply that there is no metallicity trend in

the global ratio of CO-to- H_2 in galaxies.

What about the possibility of clouds being more massive than the simple virial mass estimate? We already discussed the observation that several clouds in IC 10 and the SMC are not quite compatible with the Galactic *size-line width* relation, in the direction of too small a line width for a given size. We will argue in §5.4 that a possibility is that these clouds are transient structures not in equilibrium that will collapse in a few Myr due to the lack of turbulent support, or that they may be supported by magnetic fields in larger proportion than the typical Galactic GMC. In either case, such clouds could be removed from the sample since their line width may underestimate their true mass. Doing so slightly changes the averages for the SMC and IC 10, but does not significantly alter the results.

Thus, a consistent and uniform analysis of the available data for resolved GMCs shows no evidence for an increasing X_{CO} with decreasing metallicity. We note that this is unlike the scenario mentioned before, where similar gradients in radiation field and metallicity conspire to keep X_{CO} approximately constant in the disks of the Milky Way or M 33. Here we have galaxies (and particular GMC complexes) that simultaneously have a higher-than-Galactic radiation field and a lower-than-Galactic metallicity, yet a very similar X_{CO} for their resolved GMCs (e.g., Israel et al. 1996; Madden et al. 1997; Wilke et al. 2004).

We emphasize that these results correspond to the resolved X_{CO} . As we discussed in §5.2.2, FIR observations show that in galaxies such as the SMC, CO-bright cores are likely embedded in extended envelopes of H_2 that do not emit in CO (Madden et al. 1997; Leroy et al. 2007). The global molecular gas content of a galaxy relative to its CO luminosity may well steeply scale with its dust-to-gas ratio or metallicity, as it is strongly suggested by the available data on a few of these objects (Israel 1997; Leroy et al. 2007). Nevertheless, it appears that the structures that we are able to identify as individual GMCs by means of their CO emission have CO-to- H_2 conversion factors (as well as Larson relations) that are approximately Galactic, independent of their nebular metallicities.

We can understand the joint results from the CO and dust-continuum observations in the following terms: in a low-metallicity environment such as the SMC, CO-bright clouds are the innermost portions of considerably larger H_2 structures mostly devoid of CO emission. This scenario was suggested by Rubio et al. (1991) and Rubio et al. (1993b) for the SMC and is consistent with calculations of the effect of metallicity on the placement of the photodissociation fronts (Maloney & Black 1988; Elmegreen 1989). It also has been suggested as the situation in outer galaxy disks (Papadopoulos, Thi, & Viti 2002, but see also Wolfire et al. 2008 for a recent determination of H_2 formation rates in diffuse gas). It appears that (as described for Milky Way GMCs by Heyer & Brunt 2004) these inner portions approximately follow the Larson relations and, to CO observers capable of resolving them, they appear very similar to Galactic GMCs. Thus an approximately Galactic X_{CO} factor correctly estimates the mass of the CO-bright core, but underestimates considerably the mass of H_2 in the entire GMC. In this scenario the bulk of the mass has to be lo-

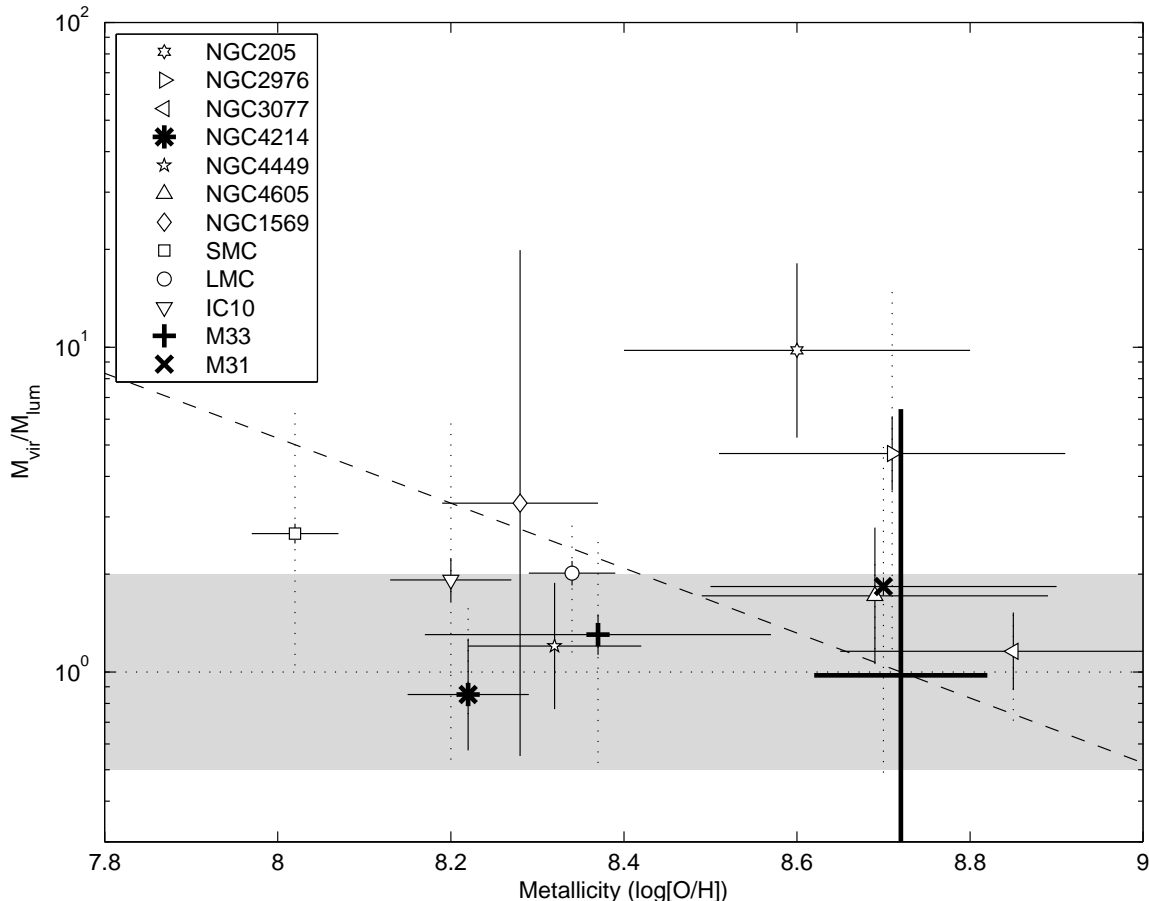


FIG. 6.— Ratio of virial to luminous mass (i.e., X_{CO} factor including the contribution from He) as a function of metallicity for the different galaxies in the sample. The ratio is normalized to the Galactic X_{CO} , as all luminous masses are computed using our adopted Milky Way value of the CO-to- H_2 conversion factor ($X_{\text{CO}} = 2 \times 10^{20} \text{ cm}^{-2} (\text{K km s}^{-1})^{-1}$, shown by the horizontal dotted line). The horizontal lines show the uncertainties in the metallicity determination, while the vertical filled lines show the uncertainties in the error-weighted X_{CO} averages in each galaxy, and the dotted lines show the range of ratios found for all clouds in each galaxy with more than one identified GMC. The gray region indicates a factor of two around Galactic X_{CO} . The symbols represent the medians for all clouds in each galaxy. The thick lines show the results for the Solomon et al. (1987) sample of Galactic clouds with masses larger than $10^5 M_{\odot}$. The dashed line illustrates $X_{\text{CO}}(Z) \propto Z^{-1}$. Note that the departure from the standard Galactic X_{CO} for the SMC is *in accordance with the Galactic relation between luminosity and virial mass* (see Equation 4). Thus it is not directly associated with metallicity, just a consequence of the smaller average mass of the SMC clouds: similar mass clouds in the inner Milky Way show the same ratio of virial to luminous mass.

cated in an envelope, surrounding the CO emission. This requires that the radiation field responsible for the photodissociation of CO be external to the cloud, and that H_2 be effective at self-shielding even in an environment with low dust-to-gas ratio and consequently reduced H_2 formation rate.

5.3. Brightness Temperatures

Column (11) in Table 3 gives brightness temperature at the cloud peak, T_B , for each GMC, a quantity set by the excitation temperature, optical depth, and filling factor of CO. Although not part of the Larson relations, this quantity is accessible in extragalactic GMCs and may yield insight into the physical state of clouds.

For Galactic clouds the average brightness temperature is ~ 4 K (Solomon et al. 1987). Many of our data exhibit notably lower T_B than this. This might indicate either lower excitation temperatures or a different optical depth of CO, due to e.g. a lower clouddlet filling factor or other geometry well below our resolution. However, the simplest explanation is that we observe GMCs with a (spatially) large beam and that beam dilution, i.e. a

low CO filling factor within the beam, lowers T_B in more distant systems.

Figure 7 shows that beam dilution indeed explains many of the the low observed T_B . We plot the mean and full range of T_B for each galaxy as a function of the spatial resolution of the data. We also show the expected T_B for the case of a uniform brightness cloud with FWHM size 40 pc (dashed line). The dashed line is consistent with most of our data, including both Local Group galaxies (the LMC, IC 10, M 33, and M 31) and more distant dwarfs (NGC 2976, NGC 4214, NGC 4605). For the more distant dwarfs, this highlights that while we resolve large (~ 100 pc) structures in the CO, these are likely blends of several GMCs.

A few extreme values of T_B cannot be immediately explained by beam dilution. NGC 3077 appears unusually bright in CO when observed with both BIMA and OVRO, perhaps a sign the that ongoing starburst at the heart of this galaxy leads to higher excitation temperatures. NGC 4449 shows a similarly high T_B . In NGC 185, NGC 205, NGC 1569, and the SMC (N83) T_B

is low despite excellent spatial resolution. In these galaxies, molecular clouds are physically smaller, have lower area filling fractions of CO emission, and/or have lower kinetic temperatures than in large galaxies. The first two might be caused by the low abundance of CO or by diminished shielding from dust as discussed in previous sections. A lower kinetic temperature remains a possibility, but is not supported by existing studies at least in the Magellanic Clouds (Bolatto, Israel, & Martin 2005). Clouds in the SMC are indeed physically smaller than in most other galaxies, but that effect does not completely account for the observed differences (see dotted line in Figure 7). This suggests that the CO emission has a lower area filling fraction: clouds in some of these galaxies are porous structures, where CO arises only from high A_V clumps.

5.4. The departures in the Small Magellanic Cloud

We discussed in §4.2 the peculiar situation of several of the least massive clouds in this study, mostly those belonging to the SMC, that systematically exhibit velocity dispersions that are too small for their sizes according to the Galactic *size-line width* relation. We noted that, despite their small sizes, these objects display exactly the opposite behavior from that observed in the outer Galaxy, where small clouds are confined by the external pressure (Heyer et al. 2001).

Under the assumption of turbulence-supported clouds in virial equilibrium following a $\sigma_v \propto R^{0.5}$ relation, the fact that many SMC and a few IC 10 clouds lie a factor of two in σ_v below the *size-line width* relation implies that their surface densities are four times lower than Galactic clouds, yielding $\Sigma_{\text{GMC}} \sim 45 \text{ M}_\odot \text{ pc}^{-2}$. Recall that, for Milky Way clouds, the observed surface density translates into a visual extinction $A_V \sim 7.5$ through the cloud. In low-metallicity galaxies such as the SMC and IC 10, where the dust-to-gas ratio is lower than in the Milky Way by at least a factor similar to their heavy-element deficit, a reduction by a factor of 4 in surface density is compounded by another factor of ~ 4 in the dust-to-gas ratio implying that we would expect extinctions of order $A_V \sim 0.5$ through the cloud, or $A_V \sim 0.2 - 0.3$ at the cloud center. We do not expect bright ^{12}CO emission at such low extinction, where most CO molecules would be photodissociated. It is possible, however, that GMCs in the SMC have a considerably lower CO area filling fraction than their Galactic counterparts. Thus, although the average surface densities and corresponding extinctions are too low to allow the formation of CO, it still exists in small, well shielded clumps within these structures. We have discussed in the previous section that there is some evidence along these lines, since clouds in the SMC indeed have lower brightness temperatures suggestive of smaller CO area filling fractions.

Alternatively, if the hypothesis of virialized clouds supported chiefly by turbulent motions is not valid, the SMC and IC 10 GMCs that fall under the *size-line width* relation show a deficit of turbulent kinetic energy with respect to similar size Milky Way clouds. Since Galactic clouds are supported against collapse by a combination of turbulence and magnetic fields with turbulence lending the main support on the large scales (McKee 1989; McKee & Ostriker 2007), this apparent deficit of turbulent energy would translate into rapid collapse and

subsequent star formation in a free-fall timescale ($t_{\text{ff}} \sim 4.4 (\bar{n}/100)^{-0.5} \text{ Myr}$, where \bar{n} is the mean volume density of the cloud; McKee 1999) unless there is significant cloud support provided by a magnetic field that is proportionally larger (or better coupled to the cloud material, perhaps due to larger cloud ionization fractions) than in otherwise similar Galactic structures.

To test this hypothesis it is necessary to obtain cloud mass determinations independent of virial assumptions. This is usually attained by employing the X_{CO} factor, modeling molecular line emission, or using measurements of the dust continuum and assuming a dust-to-gas ratio and grain emissivity. The latter method was used by Bot et al. (2007), who determined masses for several molecular clouds in the SW region of the SMC. These authors found the dust-derived masses for these clouds to be, on average, twice as large as their virial masses. Under the assumption of long-lived clouds, they attributed this fact to additional magnetic support by a $B \sim 15 \mu\text{G}$ field. This field is similar to that present in smaller structures (a few parsecs in size with masses $M < 10^3 \text{ M}_\odot$) in the Milky Way (Bertoldi & McKee 1992). Along similar lines, Leroy et al. (2007) modeling of the far-infrared emission in the SMC to derive molecular gas surface densities found a mean surface density of molecular gas $\Sigma_{\text{GMC}} = 180 \pm 30 \text{ M}_\odot \text{ pc}^{-2}$ on 46 pc scales, very similar to that observed in Milky Way GMCs. These observations suggest that surface densities in the SMC are higher than what would be implied by cloud line widths under the assumption of turbulence-supported virialized clouds.

We argued in §5.2.3 that the joint CO and dust continuum data in the SMC is best understood in terms of extended CO-faint H_2 envelopes surrounding CO-bright cores. In this interpretation, part (possibly a large part) of the mass or surface density obtained by dust continuum modeling is contributed by the extended H_2 envelope, and the mass of this envelope may not be accurately reflected in the kinematics of the CO-bright core. Consequently, the high dust-derived surface densities and low observed CO velocity dispersions may not necessarily require an enhanced magnetic support. We expect that further joint analysis of high spatial resolution FIR and CO observations will shed light on the existence of extended H_2 envelopes (Leroy et al. 2008).

6. SUMMARY AND CONCLUSIONS

We present and discuss a comprehensive set of high spatial resolution observations of CO in low mass galaxies, obtained by a combination of interferometer and single-dish instruments. Although the data are heterogeneous, we analyze them in a consistent manner to obtain GMC sizes, velocity dispersions, and luminosities. The analysis is performed using the algorithm described by Rosolowsky & Leroy (2006), which does a good job at removing the biases due to dissimilar resolution and signal-to-noise. We compare this uniform dataset of resolved extragalactic molecular cloud properties against those of GMCs in the three disk galaxies in the Local Group. To do so, we analyze the interferometric maps of M 31 (Rosolowsky 2007), M 33 (Rosolowsky et al. 2003), and the sample of Galactic GMCs discussed by Solomon et al. (1987).

The main result of this study is that, remarkably, *there*

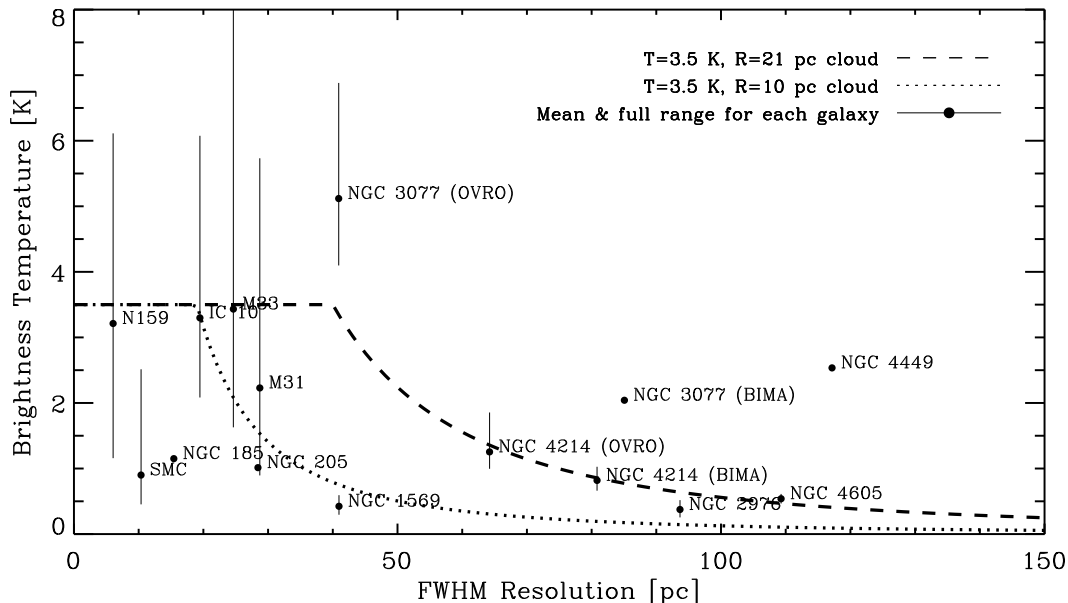


FIG. 7.— Brightness temperatures in a GMC as a function of the spatial resolution of the data set. Circles show the mean value and solid bars the full range of brightness temperatures for each galaxy. The dashed line shows the expected curve for a uniform brightness ($T = 3.5$ K) cloud with $R = 21$ pc (a typical Galactic GMC). The dotted line illustrates the expected behavior for a $R = 10$ pc cloud (a typical size for the SMC). Most galaxies are approximately compatible with the Galactic curve, but deviations exist: NGC 3077 and NGC 4449 have brighter CO than other galaxies while the SMC, NGC 185, and NGC 205 exhibit low peak temperatures even at high spatial resolution.

are only small differences between CO-bright GMCs in the Milky Way and GMCs in galaxies with metallicities as low as $0.2Z_{\odot}$ subject to a variety of physical conditions. Our sample of extragalactic GMCs follows approximately the same *size-line width*, *luminosity-size*, and *luminosity-line width* relations as Galactic clouds. Such uniformity may be in part responsible for the observed invariance of the stellar Initial Mass Function in galaxies. In any case, this result underscores that the Galactic Larson relations provide a remarkably good description of CO-bright Giant Molecular Clouds independent of their environment, at least in the range of environments explored by this study.

Although the Larson relations are approximately Galactic there are some significant departures. GMCs in dwarf galaxies tend to be slightly larger than GMCs in the Milky Way, M 31, and M 33 for a given CO luminosity or velocity dispersion. The largest departures occur in the SMC, the galaxy with the lowest metallicity of the sample. A possible interpretation, viable for most of our objects, is that GMCs in small galaxies have on average a surface density of $\Sigma_{\text{GMC}} \sim 85 \text{ M}_{\odot} \text{ pc}^{-2}$ rather than the canonical $\Sigma_{\text{GMC}} = 170 \text{ M}_{\odot} \text{ pc}^{-2}$ observed in the Galaxy. In the case of the SMC, however, the implied surface densities, and consequently the central extinction in the GMCs, would be too low to expect bright CO emission. We explore three possibilities: these clouds are transient structures not supported by turbulence and will collapse in a few Myr, or else they are supported by magnetic fields in a larger proportion than similar Galactic clouds, or maybe the kinematics of the CO cores do not reflect the presence of massive H_2 envelopes.

Analysis of the properties of our sample of extragalactic GMCs shows that they do not accord with simple

predictions from the theory of photoionization-regulated star formation (McKee 1989). In the framework of this theory, clouds in lower metallicity environments will have larger surface densities to attain similar extinction in their central regions, which can then decouple from the magnetic field and collapse. Such a trend would be evident in the coefficient of the *size-line width* relation, as expressed by Equation 13. As Fig. 5 illustrates, we see no evidence for such a trend in our data. We point out four possible caveats with these results: 1) it is possible that our observations do not probe the spatial scales on which these enhancements may occur. 2) Perhaps other parameters that enter in the theory (such as the cosmic ray ionization rate, for example) change from galaxy to galaxy in a manner that conspires to keep the coefficient of the *size-line width* relation approximately constant. 3) Maybe our identification of δ_{gr} with metallicity is incorrect and we sample a smaller range of conditions than we think we do. Or, 4) the CO kinematics do not trace the full potential of the cloud. In any case, we find a $\sigma_v R^{-0.5}$ product that is approximately constant or even decreasing for decreasing metallicity, contrary to expectations.

Finally, we address the matter of the dependency of the CO-to- H_2 conversion factor, X_{CO} , on metallicity. We find that the extragalactic GMCs in our analysis agree very well with the Galactic *luminosity-virial mass* relation. Consequently, in our study of resolved GMCs we find no measurable change of X_{CO} : over a factor of 5 in metallicity most of our galaxies are compatible with a Galactic $X_{\text{CO}} = 2 \times 10^{20} \text{ cm}^{-2} (\text{K km s}^{-1})^{-1}$ within a factor of two, and there is no discernible trend with metallicity. We emphasize, however, that this measurement is relevant on the scales of the individual, CO-

bright GMCs. Studies in the FIR and at millimeter-waves in low metallicity environments (particularly the SMC) suggest that these clouds are embedded in larger H_2 envelopes that are not traced by CO emission but contain an appreciable mass of molecular gas, at least in the case of the SMC (Israel 1997; Rubio et al. 2004; Leroy et al. 2007). These FIR results are approximately consistent with virial X_{CO} estimates obtained on larger scales than the ones discussed in this paper (Rubio et al. 1993b; Mizuno et al. 2001; Bolatto et al. 2003). We suggest that the FIR and CO observations can be simultaneously understood in the following terms: in low metallicity gas bright CO emission is relegated to the density peaks. Observations that resolve those density peaks show properties that are similar to those of Milky Way GMCs — that is the result of this study, and it is supported by studies of the structure of Milky Way GMCs (Heyer & Brunt 2004; Rosolowsky et al. 2008). On larger scales, the cloud-to-cloud velocity dispersion as well as the dust opacity suggest that there is a large mass of likely molecular material that is not accounted for by the CO intensity. Such regions would be CO-bright in objects of higher metallicity.

Studying the resolved properties of extragalactic GMCs is a challenging undertaking with the current generation of instruments, particularly for clouds in CO-

faint dwarf galaxies. In the near future the deployment of the ALMA interferometer will make it possible to obtain more precise measurements on larger samples at farther distances. Studies such as the one presented here suffer from an important bias: we can only perform them on the brightest CO peaks. The detection of clouds as faint as those in the SMC in CO, for example, is currently impossible beyond the immediate neighborhood of the Local Group. These improvements in instrumentation will soon provide powerful tests of theories of star and molecular cloud formation beyond our own Galaxy.

We thank the referee, Christine Wilson, for her thoughtful and constructive comments. We wish to thank Lisa Young, Christopher L. Taylor, Mónica Rubio, and Frank Israel for making the data on NGC 185, NGC 205, NGC 1569, LIRS36, and LIRS49 available for this study. We also want to thank Christopher McKee, Eve Ostriker, Mark Wolfire, Mark Heyer, Mark Krumholz, Mónica Rubio, Stuart Vogel, and Andrew Harris for valuable discussions and comments on drafts of this manuscript. Alberto Bolatto wishes to acknowledge partial support from the National Science Foundation grant AST-0540450.

REFERENCES

- Abgrall, H., Le Boulbot, J., Pineau Des Forêts, G., Roueff, E., Flower, D. R., & Heck, L. 1992, *A&A*, 253, 525
- Arimoto, N., Sofue, Y., & Tsujimoto, T. 1996, *PASJ*, 48, 275
- Baumgartner, W. H., & Mushotzky, R. F. 2006, *ApJ*, 639, 929
- Bell, T. A., Roueff, E., Viti, S., & Williams, D. A. 2006, *MNRAS*, 371, 1865
- Bernard, J.-Ph., et al. 2008, *AJ*, submitted
- Bertoldi, F., & McKee, C. F. 1992, *ApJ*, 395, 140
- Blitz, L., Fukui, Y., Kawamura, A., Leroy, A., Mizuno, N., & Rosolowsky, E. 2007, *Protostars and Planets V*, 81
- Bloemen, J. B. G. M., Caraveo, P. A., Hermsen, W., Lebrun, F., Maddalena, R. J., Strong, A. W., & Thaddeus, P. 1984, *A&A*, 139, 37
- Bloemen, J. B. G. M., et al. 1986, *A&A*, 154, 25
- Bohlin, R. C., Savage, B. D., & Drake, J. F. 1978, *ApJ*, 224, 132
- Bolatto, A. D., Jackson, J. M., & Ingalls, J. G. 1999, *ApJ*, 513, 275
- Bolatto, A. D., Jackson, J. M., Israel, F. P., Zhang, X., & Kim, S. 2000, *ApJ*, 545, 234
- Bolatto, A. D., Simon, J. D., Leroy, A., & Blitz, L. 2002, *ApJ*, 565, 238
- Bolatto, A. D., Leroy, A., Israel, F. P., & Jackson, J. M. 2003, *ApJ*, 595, 167
- Bolatto, A. D., Israel, F. P., & Martin, C. L. 2005, *ApJ*, 633, 210
- Boselli, A., Lequeux, J., & Gavazzi, G. 2002, *Ap&SS*, 281, 127
- Bot, C., Boulanger, F., Rubio, M., & Rantakyro, F. 2007, *A&A*, 471, 103
- Brunt, C. M. 2003, *ApJ*, 583, 280
- Brunt, C. M., & Mac Low, M.-M. 2004, *ApJ*, 604, 196
- Crutcher, R. M. 1999, *ApJ*, 520, 706
- Dame, T. M., Hartmann, D., & Thaddeus, P. 2001, *ApJ*, 547, 792
- Dib, S., & Burkert, A. 2005, *ApJ*, 630, 238
- Dickman, R. L. 1978, *ApJS*, 37, 407
- Dickman, R. L., Snell, R. L., & Schloerb, F. P. 1986, *ApJ*, 309, 326
- van Dishoeck, E. F., & Black, J. H. 1988, *ApJ*, 334, 771
- Downes, D., Solomon, P. M., & Radford, S. J. E. 1993, *ApJ*, 414, L13
- Draine, B. T., et al. 2007, *ApJ*, 663, 866
- Draine, B. T., & Bertoldi, F. 1996, *ApJ*, 468, 269
- Dufour, R. J. 1984, in *Structure and Evolution of the Magellanic Clouds*, 108, 353
- Elmegreen, B. G. 1989, *ApJ*, 338, 178
- Elmegreen, B. G., & Falgarone, E. 1996, *ApJ*, 471, 816
- Elmegreen, B. G., & Scalo, J. 2004, *ARA&A*, 42, 211
- Engargiola, G., Plambeck, R. L., Rosolowsky, E., & Blitz, L. 2003, *ApJS*, 149, 343
- Fleck, R. C., Jr. 1981, *ApJ*, 246, L151
- Gordon, K. D., Clayton, G. C., Misselt, K. A., Landolt, A. U., & Wolff, M. J. 2003, *ApJ*, 594, 279
- Grenier, I. A., Casandjian, J.-M., & Terrier, R. 2005, *Science*, 307, 1292
- Helfer, T. T., Thornley, M. D., Regan, M. W., Wong, T., Sheth, K., Vogel, S. N., Blitz, L., & Bock, D. C.-J. 2003, *ApJS*, 145, 259
- Heyer, M. H., Carpenter, J. M., & Snell, R. L. 2001, *ApJ*, 551, 852
- Heyer, M. H., & Brunt, C. M., *ApJ*, 615, L45
- Hunter, D. A. 2001, *ApJ*, 559, 225
- Hunter, D. A., Rubin, V. C., Swaters, R. A., Sparke, L. S., & Levine, S. E. 2005, *ApJ*, 634, 281
- Imara, N., & Blitz, L. 2007, *ApJ*, 662, 969
- Israel, F. P., de Graauw, T., Lidholm, S., van de Stadt, H., & de Vries, C. 1982, *ApJ*, 262, 100
- Israel, F. P., de Graauw, T., van de Stadt, H., & de Vries, C. P. 1986, *ApJ*, 303, 186
- Israel, F. P. 1988, *A&A*, 194, 24
- Israel, F. P., Maloney, P. R., Geis, N., Herrmann, F., Madden, S. C., Poglitsch, A., & Stacey, G. J. 1996, *ApJ*, 465, 738
- Israel, F. P. 1997, *A&A*, 328, 471
- Israel, F. P., Tilanus, R. P. J., & Baas, F. 2006, *A&A*, 445, 907
- Keller, S. C., & Wood, P. R. 2006, *ApJ*, 642, 834
- Kennicutt, R. C., Jr., et al. 1998, *ApJ*, 498, 181
- Kewley, L. J., & Dopita, M. A. 2002, *ApJS*, 142, 35
- Kobulnicky, H. A., Kennicutt, R. C., Jr., & Pizagno, J. L. 1999, *ApJ*, 514, 544
- Kobulnicky, H. A., & Skillman, E. D. 1996, *ApJ*, 471, 211
- Kobulnicky, H. A., & Skillman, E. D. 1997, *ApJ*, 489, 636
- Krumholz, M. R., & McKee, C. F. 2005, *ApJ*, 630, 250
- Kutner, M. L., & Leung, C. M. 1985, *ApJ*, 291, 188
- Larson, R. B. 1981, *MNRAS*, 194, 809
- Larson, R. B. 1979, *MNRAS*, 186, 479
- Lebrun, F., et al. 1983, *ApJ*, 274, 231
- Lequeux, J., Peimbert, M., Rayo, J. F., Serrano, A., & Torres-Peimbert, S. 1979, *A&A*, 80, 155
- Leroy, A., Bolatto, A. D., Simon, J. D., & Blitz, L. 2005, *ApJ*, 625, 763
- Leroy, A., Bolatto, A., Walter, F., & Blitz, L. 2006, *ApJ*, 643, 825
- Leroy, A., Bolatto, A., Stanimirovic, S., Mizuno, N., Israel, F., & Bot, C. 2007, *ApJ*, 658, 1027
- Leroy, A., Bolatto, A., Gordon, K., Stanimirovic, S., Bot, C., Israel, F., & Rubio, M. 2008, in prep.
- MacLow, M.-M. 2004, *Ap&SS*, 289, 323
- Madden, S. C., Poglitsch, A., Geis, N., Stacey, G. J., & Townes, C. H. 1997, *ApJ*, 483, 200
- Madden, S. C., Galliano, F., Jones, A. P., & Sauvage, M. 2006, *A&A*, 446, 877

- Magnani, L., Blitz, L., & Wouterloot, J. G. A. 1988, *ApJ*, 326, 909
- Maíz-Apellániz, J., Cieza, L., & MacKenty, J. W. 2002, *AJ*, 123, 1307
- Maloney, P., & Black, J. H. 1988, *ApJ*, 325, 389
- Martínez-Delgado, D., & Aparicio, A. 1998, *AJ*, 115, 1462
- McGaugh, S. S. 1991, *ApJ*, 380, 140
- McKee, C. F. 1989, *ApJ*, 345, 782
- McKee, C. F. 1999, *NATO ASIC Proc. 540: The Origin of Stars and Planetary Systems*, 29
- McKee, C. F., & Ostriker, E. C. 2007, *ARA&A*, 45, 565
- Mizuno, N., Rubio, M., Mizuno, A., Yamaguchi, R., Onishi, T., & Fukui, Y. 2001, *PASJ*, 53, L45
- Moustakas, J., & Kennicutt, R. C., Jr. 2006, *ApJ*, 651, 155
- Oka, T., Hasegawa, T., Sato, F., Tsuboi, M., Miyazaki, A., & Sugimoto, M. 2001, *ApJ*, 562, 348
- Ostriker, E. C., Gammie, C. F., & Stone, J. M. 1999, *ApJ*, 513, 259
- Padoan, P., Juvela, M., Bally, J., & Nordlund, A. 1998, *ApJ*, 504, 300
- Pak, S., Jaffe, D. T., van Dishoeck, E. F., Johansson, L. E. B., & Booth, R. S. 1998, *ApJ*, 498, 735
- Papadopoulos, P. P., Thi, W.-F., & Viti, S. 2002, *ApJ*, 579, 270
- Pilyugin, L. S., Vílchez, J. M., & Contini, T. 2004, *A&A*, 425, 849
- Piontek, R. A., & Ostriker, E. C. 2005, *ApJ*, 629, 849
- Piontek, R. A., & Ostriker, E. C. 2004, *ApJ*, 601, 905
- Richer, M. G., & McCall, M. L. 1995, *ApJ*, 445, 642
- Röllig, M., Ossenkopf, V., Jeyakumar, S., Stutzki, J., & Sternberg, A. 2006, *A&A*, 451, 917
- Rosolowsky, E., Engargiola, G., Plambeck, R., & Blitz, L. 2003, *ApJ*, 599, 258
- Rosolowsky, E., & Blitz, L. 2005, *ApJ*, 623, 826
- Rosolowsky, E., & Leroy, A. 2006, *PASP*, 118, 590
- Rosolowsky, E. 2007, *ApJ*, 654, 240
- Rosolowsky, E., & Simon, J. D. 2007, *ApJ*, in press (arXiv:0711.4351)
- Rosolowsky, E. W., Pineda, J. E., Kauffmann, J., & Goodman, A. A. 2008, *ApJ*, in press (arXiv:0802.2944)
- Rubio, M., et al. 1993a, *A&A*, 271, 1
- Rubio, M., Garay, G., Montani, J., & Thaddeus, P. 1991, *ApJ*, 368, 173
- Rubio, M., Lequeux, J., & Boulanger, F. 1993b, *A&A*, 271, 9
- Rubio, M., Boulanger, F., Rantakyro, F., & Contursi, A. 2004, *A&A*, 425, L1
- Sakai, S., & Madore, B. F. 2001, *ApJ*, 555, 280
- Salaris, M., & Cassisi, S. 1998, *MNRAS*, 298, 166
- Sanders, D. B., Clemens, D. P., Scoville, N. Z., & Solomon, P. M. 1986, *ApJS*, 60, 1
- Sanders, D. B., Solomon, P. M., & Scoville, N. Z. 1984, *ApJ*, 276, 182
- Sawada, T., et al. 2001, *ApJS*, 136, 189
- Sheth, K., Vogel, S. N., Wilson, C. D., & Dame, T. M. 2008, *ApJ*, in press (arXiv:0710.4559)
- Simon, R., Jackson, J. M., Clemens, D. P., Bania, T. M., & Heyer, M. H. 2001, *ApJ*, 551, 747
- Simon, J. D., Bolatto, A. D., Leroy, A., & Blitz, L. 2003, *ApJ*, 596, 957
- Skillman, E. D. 2003, in “Star Formation Through Time”, E. Pérez, R.M. González Delgado, and G. Tenorio-Tagle eds., *ASP Conference Series Vol. 297*, 121
- Skillman, E. D., Kennicutt, R. C., & Hodge, P. W. 1989, *ApJ*, 347, 875
- Sodroski, T. J., et al. 1995, *ApJ*, 452, 262
- Solomon, P. M., Rivolo, A. R., Barrett, J., & Yahil, A. 1987, *ApJ*, 319, 730
- Stanimirović, S., Staveley-Smith, L., van der Hulst, J. M., Bontekoe, T. R., Kester, D. J. M., & Jones, P. A. 2000, *MNRAS*, 315, 791
- Stone, J. M., Ostriker, E. C., & Gammie, C. F. 1998, *ApJ*, 508, L99
- Strong, A. W., & Mattox, J. R. 1996, *A&A*, 308, L21
- Taylor, C. L., Kobulnicky, H. A., & Skillman, E. D. 1998, *AJ*, 116, 2746
- Taylor, C. L., Hüttemeister, S., Klein, U., & Greve, A. 1999, *A&A*, 349, 424
- Vogel, S. N., Boulanger, F., & Ball, R. 1987, *ApJ*, 321, L145
- Vermeij, R., & van der Hulst, J. M. 2002, *A&A*, 391, 1081
- Vestuto, J. G., Ostriker, E. C., & Stone, J. M. 2003, *ApJ*, 590, 858
- Walter, F., Taylor, C. L., Hüttemeister, S., Scoville, N., & McIntyre, V. 2001, *AJ*, 121, 727
- Walter, F., Weiß, A., Martin, C., & Scoville, N. 2002, *AJ*, 123, 225
- Walter, F., 2003, *Proceedings of the 4th Cologne-Bonn Zermatt Symposium “The Dense Interstellar Medium in Galaxies”*
- Weiß, A., Neininger, N., Hüttemeister, S., & Klein, U. 2001, *A&A*, 365, 571
- Welch, W. J. et al. 1996, *PASP*, 108, 93
- Wilke, K., Klaas, U., Lemke, D., Mattila, K., Stickel, M., & Haas, M. 2004, *A&A*, 414, 69
- Wilson, C. D. 1995, *ApJ*, 448, L97
- Wilson, C. D., & Scoville, N. 1990, *ApJ*, 363, 435
- Wolfire, M. G., Hollenbach, D., & Tielens, A. G. G. M. 1993, *ApJ*, 402, 195
- Wolfire, M. G., Tielens, A. G. G. M., Hollenbach, D., & Kaufman, M. J. 2008, *ApJ*, 680, 384
- Yao, L., Seaquist, E. R., Kuno, N., & Dunne, L. 2003, *ApJ*, 588, 771
- Young, L. M. 2001, *AJ*, 122, 1747